energies

MDPI

Article

Development of Sky Luminance and Daylight Illuminance Prediction Methods for Lighting Energy Saving in Office Buildings

Chul-Ho Kim and Kang-Soo Kim *

Department of Architecture, College of Engineering, Korea University, 145 Anam–Ro, Seongbuk-Gu, Seoul 02841, Korea; kchcd@korea.ac.kr

* Correspondence: kskim@korea.ac.kr; Tel.: +82-2-3290-3744

Received: 7 January 2019; Accepted: 11 February 2019; Published: 13 February 2019

Abstract: Accurately predicting indoor illuminance from daylight during the early stages of building design is an important factor in saving energy and the costs associated with lighting. The objective of this study was to predict sky luminance distribution using the Commission Internationale de l'éclairage (CIE) standard sky model, and propose a method that can be used to predict indoor illuminance. Results obtained from the proposed prediction method were compared and verified with simulation values obtained by Desktop Radiance. From the CIE overcast sky, the zenith/horizon ratio was 3:1. From the CIE clear sky, the luminance value was highest around the sun. In contrast, the luminance value was lowest in the opposite direction of the sun when the angle between the sun and sky elements was 90°. In addition, this study suggested an indoor illuminance prediction method by applying the effects of sky luminance, direct sunlight, and wall reflection elements. When the proposed equation's calculation results were compared with Desktop Radiance simulation's value in overcast and clear sky, all statistically analysis (R^2, MBE, Cv(RMSE), *t*-value, *p*-value) satisfied each standard and showed high correlations. Consequently, it was established that the predicted indoor illuminance obtained from the proposed prediction method was accurate and can be used to predict the level of indoor illuminance. The results further revealed that it is possible to calculate indoor illuminance when installing blinds, by substituting variable values of visible light transmittance (VLT).

Keywords: prediction method; sky luminance; daylight illuminance; delight algorithm; CIE standard clear sky; CIE standard overcast sky; lighting energy; desktop radiance

1. Introduction

1.1. Background and Purpose

Daylight is an important factor that influences building lighting energy efficiency and visual satisfaction for the occupants [1,2]. Accurate estimation of indoor daylight illuminance is important in saving lighting energy, as indoor daylight illuminance data can be used to predict a building's lighting energy and improve energy efficiency. Especially in a general office building, lighting energy consumption is responsible for 20%–30% of the total building energy consumption [3–6], and the effective control of daylight can reduce lighting energy consumption by 30%–60% annually [7–9].

Sky luminance distribution greatly affects the indoor illuminance making the prediction of sky luminance distribution very important [10–12]. In other words, we should first predict and evaluate the sky luminance distribution to accurately predict indoor daylight illuminance. As sky luminance can vary considerably, we should have an accurate standard to derive an objective conclusion [13].

The Commission Internationale de l'Eclairage (CIE) [14] provides a universal standardized method for calculating sky luminance in daylighting prediction procedures for the classification of measured sky luminance distributions [15]. These types of sky luminance models are useful for predicting indoor daylight illuminance and lighting control strategies, making it possible to improve lighting energy efficiency. Evaluation facilities that realize sky luminance distribution include the sky simulator, artificial sky dome, and sky scanner [16–19]. However, these facilities can be costly and require a significant amount of user expertise. Thus, a theoretical study is necessary to develop an algorithm that can easily create sky luminance for illuminance predictions.

The primary aim of this study is to first construct an algorithm outline for the creation of sky luminance distribution through a theoretical study of CIE's general sky model [20–25] to make luminance prediction cost–effective, realize CIE overcast sky and clear sky's luminance distribution, and verify the luminance distribution by comparing it with Desktop Radiance [26–30] simulation results. Secondly, to formulate an indoor illuminance prediction equation derived from the DeLight algorithm [31–34] by applying the effects of sky luminance, direct sunlight, and wall reflection elements and to suggest a method for accurately predicting indoor daylight illuminance during the daylighting design procedures.

1.2. Literature Review

Various studies have focused on sky luminance and indoor daylight illuminance with an aim of improving the lighting energy efficiency of buildings.

Standard general sky guide [21] collected information for the application of the CIE standard general sky for general users and designers. The guide provided an explanation to the CIE standard general sky concept, which is described in ISO 15469:2004/CIE S 011:2003, and its simplified use by practitioners. The document includes an extensive list of references on the subject and gives recommendations on prediction methods, tools, and computer programs.

Kittler and Darula [22–25] studied the International Organization for Standardization/ Commission Internationale de l'Eclairage (ISO/CIE) sky classifications to improve the accuracy in predictions of indoor daylight illuminance in the initial stages of building design. Their study also calculated standardized relative luminance distributions for each type of sky from the zenith luminance to the horizontal level. The ISO/CIE sky classifications are presently standardized as relative luminance patterns normalized to the zenith. In their paper, the zenith luminance and the resulting skylight horizontal diffuse illuminance in, respectively, units of cd/m^2 and lx are determined for all sky types. Furthermore, the proportions of sunlight and skylight under different levels of turbidity are documented.

Tregenza [35] studied the 15 sky luminance models using data recorded at four stations: Singapore (1.5N and 103.8E), Fukuoka (Japan, 33.5N and 130.5E), Garston (United Kingdom, 51.7N and 0.4W) and Sheffield (UK, 53.5N and 1.5W) representing tropical humid and temperate maritime climates. Tregenza concluded that the standard set of sky types provides a good overall framework for categorizing actual sky conditions, and the subset of four luminance distributions proved adequate to describe the sky conditions appearing at each station. In another study, Tregenza [36] classified the standard skies, and the luminance distributions of individual standard sky types were modeled and compared with recorded data in terms of the root–mean–square error (RMSE).

Enarun and Littlefair [37] measured the overcast sky luminance distributions in a region in southern England using a sky scanner. They then compared their measurements against models published by the CIE, Perez, Commbes and Harrison, Muneer and Angus, Perraudeau, Hooper and Brunger's. They reported that the CIE overcast sky classification most accurately described the fully overcast sky luminance distribution of southern England.

Li et al. [38,39] also found that the CIE standard overcast sky matched well with overcast sky luminance distribution data measured in Hong Kong. They created a database of Hong Kong's actual measure of solar radiation and sky luminance distribution with overcast skies for the sake of evaluating

indoor visual environments. Chirarattananon and Chaiwiwatworakul [40] measured sky luminance at North Bangkok mainly under clear and intermediate skies. They then evaluated indoor illuminance and visual environments with a detailed analysis of Bangkok's actual sky luminance distribution under overcast conditions.

Igawa et al. [41] proposed models of radiance and sky luminance distributions for all sky conditions from clear to overcast. They classified sky luminance distributions of Tokyo's various sky conditions into indices of clear and cloudless skies. They then analyzed these distributions and compared them against various existing sky model theories. Li and Lou [42] compared non–overcast sky luminance models with data recorded in Hong Kong. They found that sky luminance distributions are affected by various factors, such as the sun's position, turbidity and pollution content in the atmosphere, and the amount, type, and pattern of cloud cover.

Bartzokas et al. [43] studied the sky luminance levels Bratislava, Central Europe and Athens, on the Eastern Mediterranean coast. They defined the prevailing sky luminance distributions for winter and summer. These prevailing sky luminance distributions were intended for use in the design of building openings to increase energy efficiency.

Wittkopf and Soon [44] studied three methods for sky distribution analysis: classification with the relative indicatrix and gradation, along with two independent methods established by Kittler and Tregenza. All three methods were verified to be used for analyzing the extreme daylight conditions in Singapore, which is located at the equator. They found that the analysis of sky distributions is useful for the prediction of daylight patterns and can guide the design of architectural windows and building envelopes.

Numerous studies have been done with respect to indoor daylight illuminance predictions using various methods. Additionally, some studies explain the importance of scale models in artificial and real skies. Navvab [45,46] studied the application of scale models in the prediction of daylight illumination in buildings. In order to measure indoor illuminance, the scale models are used under real sky or simulated sky conditions. In their studies, Navvab reported on the use of scale model in comparative evaluation of model photometry and computer simulation. The scale model provided an increase in the accuracy of the assessment in simplified methods. They explained that scale models are used as an accurate method to evaluate the design performance or to identify a relationship between a proposed design and its elements under real conditions. Navvab et al. [47] also studied the estimated frequencies of CIE luminance distributions and the impact of circumsolar region using TMY weather files, a typical meteorological year (TMY). The TMY can be used to provide hourly results at any location where a TMY or an irradiance time series is available.

Gugliermetti and Bisegna [48] presented simplified algorithms for assessing the indoor daylight illuminance on a prefixed point using external fixed shading devices in various Mediterranean cities. The proposed method in their study was based on splitting the internal illuminance into two components; due to direct and diffuse sun radiations, expressed by the Solar System Luminous Efficacies (SSLEs) and calculated using the package Superlite. SSLEs correlations were tested using experimental measurements on scale models.

In addition, Gugliermetti and Bisegna [49] analyzed the office demand associated with the use of different dynamic window (electrochromic windows) and lighting control systems with the aim of optimizing their usage aspects and characteristics from both visual and energy efficiency point of view. They used the hourly simulation program IENUS (Integrated ENergy Use Simulation). Different electrochromic windows and light management strategies were adopted in their Mediterranean climate studies using TMY weather files.

Tregenza [50] developed a tool for estimating the indoor horizontal illuminance of windows facing large external obstructions under the traditional CIE overcast sky, with a modification of the split–flux formula. Tregenza [51] also formulated simple calculation procedures for determining the indoor daylight illuminance in rooms facing sunlit streets. He described a method for estimating the

mean illuminance on the working plane and on other room surfaces from data about the normal solar illuminance and diffuse horizontal illuminance.

Li et al. [52] suggested a nomograph and a formula for predicting indoor horizontal illuminance that consider indoor reflective components and sky models during initial design stages of a building. They verified the results by comparing them with actual measurements of a scaled–down model.

Li et al. [53] also studied Desktop Radiance program simulation approaches, then compared its results with the indoor daylight illuminance measured in a scale model and in a classroom. In general, the daylight–factor (DF) approach is simple, but it cannot predict dynamic variations in indoor horizontal illuminance that follow changes in sky conditions and the sun's position. With the constant advancement in computer technology, the daylight illuminance can be predicted effectively using Desktop Radiance simulation software.

Vartiainen [31] suggested a formula for predicting daylight illuminance at a particular position indoors. The prediction results were compared against actual measured illuminance, showing that illuminance is more predictable on overcast days with no direct sunlight. However, daylight illuminance is much less predictable with this method if the point is exposed to direct sunlight.

Yoon et al. [54] came up with a simplified equation for evaluating daylight factors in overcast conditions using measured values of vertical illuminance in Seoul, Korea. The results were compared with measurements of a 1/5–scale model room to evaluate the precision of the suggested equation.

Although numerous studies were carried out as shown, methods for predicting sky luminance, such as the sky simulator, artificial sky dome, and sky scanner, were costly. Methods used for predicting indoor daylight illuminance were either using computer software which requires expert knowledge, or using expensive equipment for experimental studies.

Therefore, this study sought to construct an algorithm framework for sky luminance distribution without relying on costly equipment through CIE general sky model theory evaluation; it also utilized the CIE general sky algorithm for indoor illuminance prediction. In addition, it was determined that there is a need for a study that can improve indoor illuminance predictability via a theoretical approach to the prediction formula without relying on costly computer simulation methods that require user expertise.

1.3. Method and Process

1.3.1. Selection for Verification Program (Desktop Radiance)

Desktop Radiance [26] was used to check the prediction equation proposed in this study. It was ordered from U.S.A Department of Energy (DOE) and developed at the Lawrence Berkeley National Laboratory (LBNL). This program has been verified through numerous studies, and the program makes it possible to simulate a wide range of visual environments [26–30]. In addition, it is possible to calculate illuminance of space using illuminance sensors, then compare its results from those of predicted equation.

1.3.2. Calculation and Verification of Sky Luminance Distribution

Thus, to calculate sky luminance distribution, the CIE standard sky luminance distribution provided by CIE [14] and a theory regarding the CIE general sky standard [20–23] were examined. The sky luminance distribution of CIE overcast and CIE clear sky was reproduced with 145 sky luminance patches [36] through the algorithm of sky luminance distribution. CIE overcast sky and CIE clear sky luminance distributions were compared with Desktop Radiance simulation results for verification.

1.3.3. Evaluation on daylight illuminance using modified daylight prediction equation

In this study, the DeLight daylight algorithm [31–34] was analyzed to obtain a modified daylight prediction equation. For a more accurate indoor illuminance prediction, sky luminance, simulation model data, and indoor–reflected components of model were integrated into a modified formula.

The modified formula was then used to compare the indoor illuminance prediction values for CIE overcast sky and CIE clear sky with the Desktop Radiance [26–30] simulation results for verification. The daylight factor (DF), a ratio of indoor illuminance to overall sky luminance, was also divided into its sky component (SC) and internally reflected component (IRC) for comparison of CIE overcast sky conditions. For CIE clear sky conditions, the simulation model was unfolded in six directions and evaluated with luminance distribution. The indoor illuminance distribution when external blinds are installed was also evaluated. Figure 1 shows a flow chart of the study process.

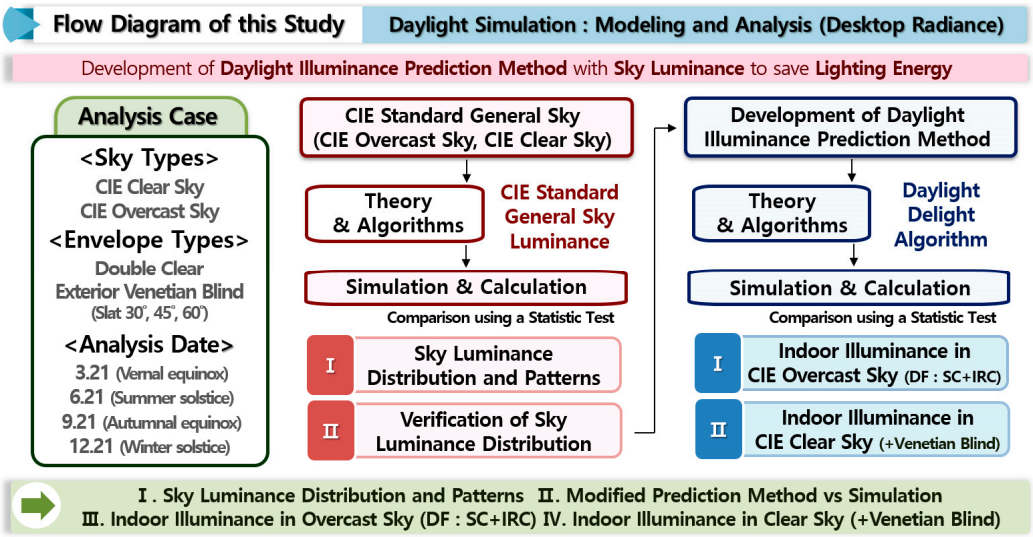

Figure 1. Flow diagram of this study.

2. Theory

2.1. CIE Standard Sky Model

2.1.1. CIE Standard Overcast Sky

The Northern European countries such as the UK and Scandinavia frequently experience overcast sky. CIE selected the overcast sky as a standard design sky to calculate illuminance, which displays an irregular distribution having a zenith to horizon ratio of 3:1. Equation (1) [15,39,55] expresses the rate of division between luminance of a sky element and zenith luminance for an overcast sky:

$$\frac{L_\gamma}{L_Z} = \frac{1+2\sin\gamma}{3} = \frac{1+2\cos Z}{3} \quad (1)$$

where L_γ = Luminance of a sky element (kcd/m^2), L_z = the zenith luminance (kcd/m^2), γ = the elevation angle of a sky element above the horizon and Z = the angular distance between a sky element and the zenith.

2.1.2. CIE Standard Clear Sky

The CIE clear sky model assumes that luminance is highest near the Sun and lowest near the sky perpendicular to the position of the Sun. The elevation angle and azimuth of SC and the Sun are important variables for CIE clear sky's luminance distribution. Kittler's equation is commonly referred to as the luminance equation for a clear sky, which is expressed as shown in Equation (2) [15,56]:

$$\frac{L_{\gamma\alpha}}{L_Z} = \frac{(1-e^{-0.32/\sin\gamma})(0.91+10e^{-3\chi}+0.45\cos^2\chi)}{0.274(0.91+10e^{-3Z_s}+0.45\cos^2 Z_s)} \quad (2)$$

where $L_{\gamma\alpha}$ = luminance in any arbitrary sky element, χ = the angular distance of the sky element from the Sun and Z_s = the zenith distance of the Sun.

2.1.3. The CIE General Sky Standard (Kittler's model)

From the ISO 15469/2004 standard [20], CIE general sky is classified into two groups: indicatrix and gradation. CIE general sky is also divided into different classifications and includes sky luminance distribution in Kittler's study [22–25]. The position of the Sun, the arbitrary sky element, and parameters a, b, c, d, and e, which describe atmospheric conditions, are used as input calculation quantities. For window design, glare studies, energy analysis, daylight climate classifications, and other purposes, parameters a, b, c, d and e used in the equations can be selected from Table 1, which lists five standard relative luminance distributions that are based on six groups of a and b values for the gradation function and six groups of c, d, and e values for the indicatrix function.

Table 1. CIE standard sky model's parameters.

Type	Gradation	Indicatrix	a	b	c	d	e	Description of Luminance Distribution
1	**I**	**1**	4.0	−0.7	0	−1.0	0.00	CIE Standard Overcast Sky, Alternative form steep luminance gradation towards zenith, Azimuthal uniformity
2	**I**	**2**	4.0	−0.7	2	−1.5	0.15	Overcast Sky, with steep luminance gradation and slight brightening towards the Sun
5	**III**	**1**	0.0	−1.0	0	−1.0	0.00	Sky of Uniform Luminance
6	**III**	**2**	0.0	−1.0	2	−1.5	0.15	Partly Cloudy Sky, No gradation towards zenith, Slight brightening towards the Sun
12	**V**	**4**	−1.0	−0.32	10	−3.0	0.45	CIE Standard Clear Sky, Low illuminance turbidity
13	**V**	**5**	−1.0	−0.32	16	−3.0	0.30	CIE Standard Clear Sky, polluted atmosphere

Figure 2 presents a diagram of sky relative luminance distribution based on the location of the sun and arbitrary sky elements. The ratio of the luminance $L_{\gamma\alpha}$ in an arbitrary sky element to the zenith luminance L_z is expressed as shown in Equation (3) following the current CIE clear sky standard [15,21,23–25]:

$$\frac{L_{\gamma\alpha}}{L_z} = \frac{f(\chi)\phi(Z)}{f(Z_s)\phi(0^\circ)} \tag{3}$$

where $L_{\gamma\alpha}$ = luminance in any arbitrary sky element and L_γ = luminance of a sky element (kcd/m^2).

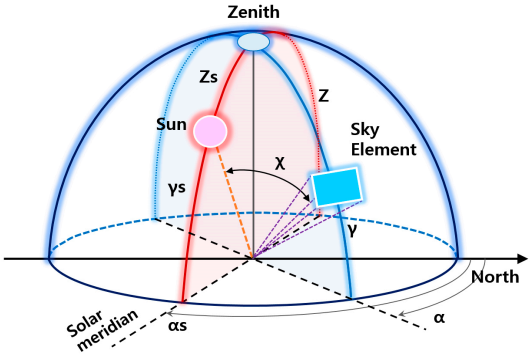

Figure 2. Diagram showing the position of the sun and sky element.

The position of the arbitrary sky element is defined by the zenith angle Z and the azimuth difference A_z between the element and the solar meridian, as shown in Figure 2, then its distance from the sun can be found using Equation (4) [15,21,25]:

$$\chi = \arccos\left(\cos Z_s \cos Z + \sin Z_s \sin Z \cos A_z\right) \tag{4}$$

where $A_z = |\alpha - \alpha_s|$ α and α_s are azimuthal angles of the vertical plane of the sky element and Sun position, respectively.

The function $f(\chi)$ (Equation (5)) expresses the scattering indicatrix, which relates the relative luminance of a sky element to its angular distance from the Sun [15,21,25]:

$$f(\chi) = 1 + c(\exp(dx) - \exp(d\pi/2)) + \mathrm{e}\cos^2\chi \tag{5}$$

where χ = the angular distance of the sky element from the Sun.

The function $f(Z_s)$ expresses the scattering indicatrix which relates the relative luminance of the zenith distance of the sun. Its value at the zenith is expressed in Equation (6) [15,21,25]:

$$f(Z_s) = 1 + c(\exp(dZ_s) - \exp(d\pi/2) + e\cos^2 Z_s \tag{6}$$

where Z_s = The zenith distance of the Sun.

The luminance gradation function ϕ relates the luminance of a sky element to its zenith angle, as expressed in Equation (7) [15,21]:

$$\phi(Z) = 1 + \mathrm{a}\ \exp(b/\cos Z),\ \phi(0^\circ) = 1 + a\exp b \tag{7}$$

where when $0 \le Z \le \pi/2$, and at the horizon, $\phi(\pi/2) = 1$.

By using the formal study of Kittler [15,21–25], the zenith luminance and sky luminance, which were based on the data collected from the illuminance sensor, can be calculated. Each coefficient values (A, B, C, D, E, and T_v) were proposed in the prior study. Darula and Kittler [15] explain that one can apply Equation (8) to skies with luminous turbidity factor (T_v) value greater than 12 and Equation (9) to clear skies with T_v value lower than 12:

$$L_z = \frac{D_v}{E_v}\left[\frac{B(\sin\gamma_s)^C}{(\cos\gamma_s)^D} + \mathrm{Esin}\gamma_\mathrm{s}\right](\mathrm{kcd/m^2}) \tag{8}$$

where E_v = extraterrestrial horizontal illuminance, L_z = the ratio of zenith luminance to diffuse sky illuminance D_v and γ_s = elevation angle of the Sun:

$$\begin{gathered} A = (\mathrm{A1}T_v + \mathrm{A2}) \\ L_z = \mathrm{Asin}\gamma_s + 0.7(T_v + 1)\frac{(\sin\gamma_s)^C}{(\cos\gamma_s)^D} + 0.04T_v \end{gathered} \tag{9}$$

where A, B, C, D, and E = parameters characterizing a certain sky standard and T_v = the luminous turbidity factor.

Figure 3 shows the flow of the algorithm explained above for the realization of CIE overcast and clear skies' luminance distribution i.e. one can derive an equation that comprises Equation (3) and the resulting values from Equations (4)–(7) from the Sun and the sky's position (altitude, azimuth). The result can be used to derive the ratio between zenith luminance and sky luminance. Also, the sun's position (altitude, azimuth) can be incorporated into Equations (8) and (9) to derive the zenith luminance of overcast sky and clear sky. Each sky model's luminance can be obtained by multiplying Equation (3) by the results from Equations (8) and (9), respectively. The detailed results are presented in Section 4.

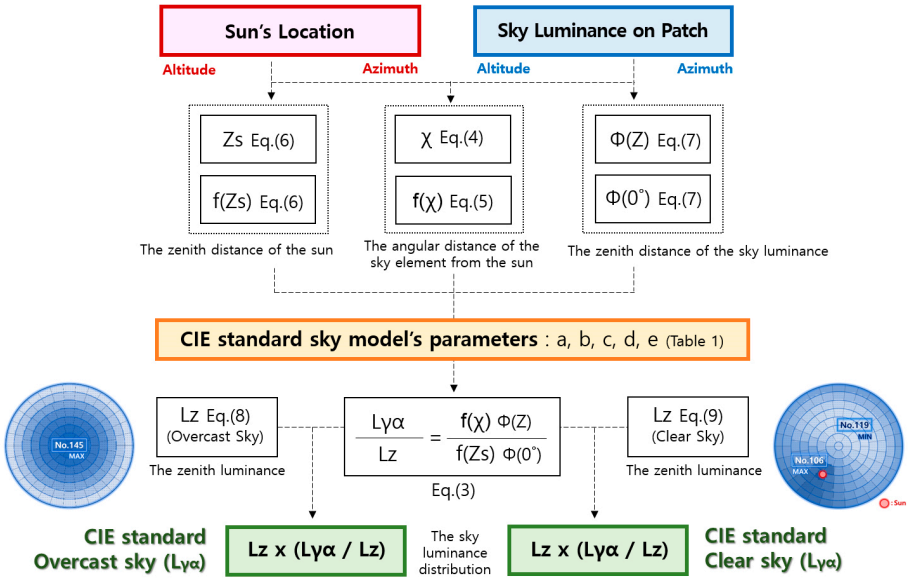

Figure 3. Algorithm framework of sky luminance distribution.

2.2. *Suggestion of the Daylight Illuminance Prediction Equation*

Suggestion of the Daylight Prediction Equation using the DeLight Algorithm

The DeLight algorithm suggests an indoor diffuse illuminance distribution equation, as shown in Equation (10) [31,32] using the position index in Figure 4.

$$E_{p,d} = \frac{r_w L}{2} \times \frac{z}{\sqrt{{h_p}^2+z^2}} \left(\tan^{-1} \frac{x_w+w_w-x_p}{\sqrt{{h_p}^2+z^2}} + \tan^{-1} \frac{x_p+x_w}{\sqrt{{h_p}^2+z^2}} \right) - \frac{z}{\sqrt{(h_p+h_w)^2+z^2}} \left(\tan^{-1} \frac{x_w+w_w-x_p}{\sqrt{(h_p+h_w)^2+z^2}} + \tan^{-1} \frac{x_p-x_w}{\sqrt{(h_p+h_w)^2+z^2}} \right) \quad (10)$$

where $E_{p,d}$ = indoor horizontal diffuse illuminance at P point (lx), L = sky luminance (the center of the part of the sky visible to point P through the window) (kcd/m^2), z = the distance between the window and P point (m), h_p = height between lower edge of the window and P point (m), h_w = window height (m), W_w = window width (m), X_w = distance between the left edge of the window and left wall (m) and X_p = distance between the reference point P and left wall (m).

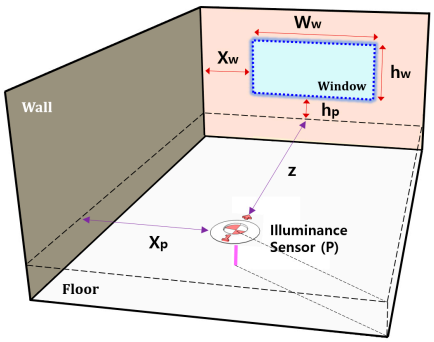

Figure 4. Room geometry for calculating the indoor horizontal illuminance.

Equation (11) [31] considers influence of reflected components from the back wall:

$$E_{p,r} = \frac{r_w L}{2} \times \left(\frac{h_w}{\sqrt{{h_w}^2 + z^2}} \tan^{-1} \frac{w_w}{\sqrt{{h_w}^2 + z^2}} + \frac{w_w}{\sqrt{{w_w}^2 + z^2}} \tan^{-1} \frac{h_w}{\sqrt{w_w + z^2}} \right) \tag{11}$$

where $E_{p,r}$ = indoor horizontal reflected illuminance at P point (lx), τ_w = visible light transmittance, L = center of window luminance (kcd/m^2), z = the distance between the window and P point (m), h_w = window height (m) and W_w = window width (m).

Equations (12) and (13) [31,32] are direct component equations, which modify the incidence angle through the window:

$$E_{p,b} = \tau_w(\theta_i) E_b \tag{12}$$

$$E_b = K_b G_b \tag{13}$$

where $E_{p,b}$ = indoor horizontal beam illuminance at P point (lx), τ_w = visible light transmittance of glazing and blinds, θ_i = an incidence angle, E_b = horizontal beam illuminance measured outdoors (lx), K_b = luminous efficacy of the beam radiation (lm/W) and G_b = outdoor horizontal beam radiation (W/m^2).

Visible light transmittance (VLT) of the blind and window can be defined using Equation (14) [57] shown below:

$$\tau_w(\theta_i) = 1.018 \tau_w(0) \cos\theta_i (1 + \sin^3 \theta_i) \tag{14}$$

where $\tau_w(0)$ = light transmittance of window with the angle of incidence 0° and θ_i = an incidence angle.

Equation (15) defines the location of the Sun and azimuth of the window [32]:

$$\cos\theta_i = \cos\theta_s \times \cos(\psi_s - \psi_w) \tag{15}$$

where θ_s = Sun's altitude (rad), Ψ_s = Sun's azimuth (rad) and Ψ_w = window surface azimuth (rad).

Suggested Equation (16) shows the influence of reflected components of all interior walls. The previous equation was limited because it only considered reflected components from the back wall. Therefore, the modified equation includes reflective components from all interior walls:

$$\begin{aligned} E_{p,rn} = \; & \tfrac{r_w L}{2} \cdot \rho_s \cdot R_f \left(\tfrac{h_w}{\sqrt{{h_w}^2 + z^2}} \tan^{-1} \tfrac{w_w}{\sqrt{{w_w}^2 + z^2}} + \tfrac{w_w}{\sqrt{{w_w}^2 + z^2}} \tan^{-1} \tfrac{h_w}{\sqrt{w_w + z^2}} \right) + 2 \tfrac{r_w L}{2} \\ & \cdot \rho_s \cdot R_f \left(\tfrac{w_w}{\sqrt{{w_w}^2 + z^2}} \tan^{-1} \tfrac{h_w}{\sqrt{{h_w}^2 + z^2}} + \tfrac{h_w}{\sqrt{{h_w}^2 + z^2}} \tan^{-1} \tfrac{w_w}{\sqrt{h_w + z^2}} \right) \end{aligned} \tag{16}$$

where $E_{p,r}$ = Indoor horizontal reflected illuminance at P point (lx), τ_w = visible light transmittance, L = center of window luminance (kcd/m^2), z = the distance between the window and P point (m), h_w = window height (m), W_w = window width (m), R_f = average indoor surface reflectance (%) and ρ_s = ground surface reflectance (%).

Overall, modified daylight prediction E_p considers three factors, the direct component, the sky diffuse component, and the reflected component, which are all employed in Equation (17). When there is an overcast or clear sky without a direct solar component, E_p can be calculated except $E_{p,b}$:

$$E_p = E_{p,b} + E_{p,d} + E_{p,rn} \tag{17}$$

Figure 5 shows the flow of the algorithm for predicting the indoor daylight illuminance in CIE overcast and CIE clear sky conditions. The calculation for indoor daylight illuminance of each sky continues from the algorithm flow shown in Table 2 and Figure 5 and uses the equations described throughout this section in conjunction with sky luminance, spatial position data, and the position of the sun. The detailed results are presented in Section 5.

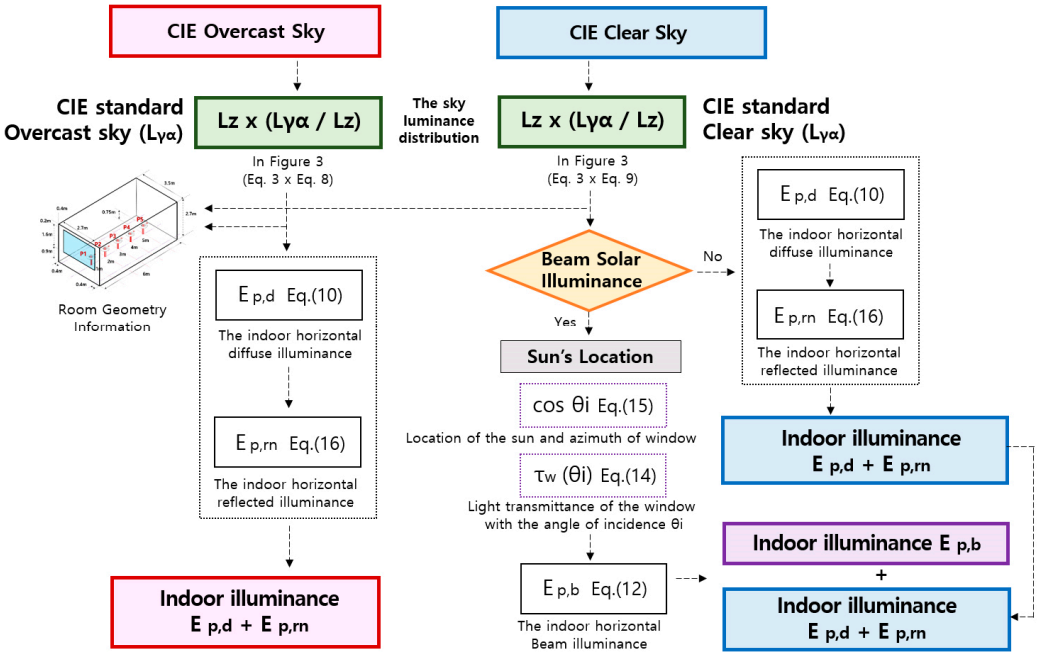

Figure 5. Diagram used in calculating the indoor illuminance in CIE clear and overcast sky.

Table 2. Comparison of DeLight algorithm and suggested daylight algorithm.

Algorithm	Diffuse Illuminance Components	Direct Illuminance Components	Reflected Illuminance Components	Total Indoor Illuminance (Ep)
DeLight Algorithm [31–34]	Equation (10) ($E_{p,d}$)	Equations (12–15) ($E_{p,b}$)	Equation(11) ($E_{p,r}$)	$E_{p,d} + E_{p,b} + E_{p,r}$
Suggested Daylight Algorithm	Equation (10) ($E_{p,d}$) using sky luminance in Figure 3	Equations (12–15) ($E_{p,b}$)	Equation(16) ($E_{p,rn}$) considering reflectivity of all interior walls	Equation (17) $E_{p,d} + E_{p,b} + E_{p,rn}$

3. Simulation Analysis Model and Conditions

3.1. Simulation Analysis Model and Sensors

Figure 6 shows information of the analysis model. This model was used to perform a simulation and apply modified daylight prediction.

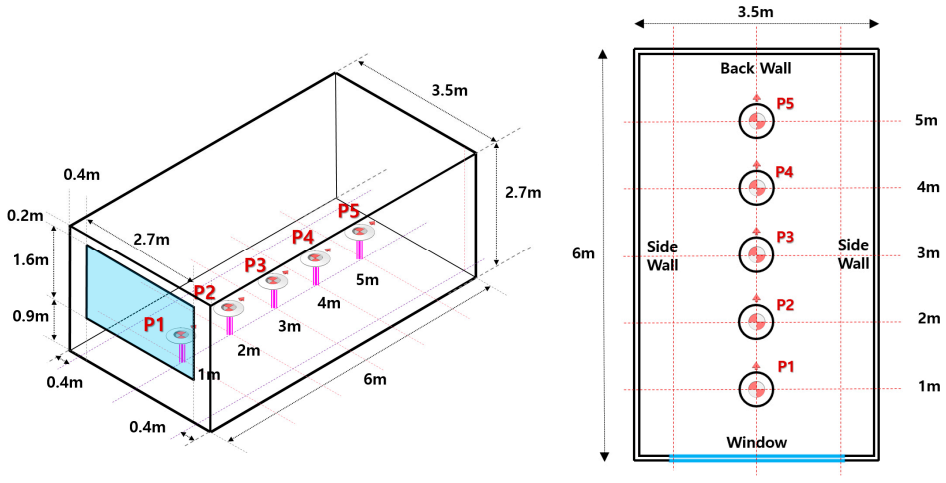

Figure 6. Simulation model and illuminance sensors installation.

An analysis model was set as the evaluation space with a model size width of = 3.5 m, depth = 6 m, and ceiling height = 2.7 m, and the window to wall ratio (WWR) of 45%, excluding the frame because it could result in an irregular indoor illuminance value. "Window design Guidelines for Building Energy Conservation" published by Korean Ministry of Land, Infrastructure and Transport (MOLIT) [58] suggests the WWR to be 40–50%. Thus, we set the WWR of the analysis model as 45%. Also, the room ratio (room length/width) [59] of the scale model that we are currently making for future experiments study as the analysis model's room ratio. To measure the illuminance of the evaluation space at each measurement point, a total of five (1 × 5) sensor grids were installed at a height of 0.75 m with an interval of 1 m.

Table 3 provides the finishing material's model reflection rate, which included the ceiling (85%), the wall (55%), the floor (20%), and the window (5%), with a window transmittance of 78%. Using these values, the average indoor surface reflection rate was estimated to be 55%.

Table 3. Properties of simulation model.

Surface of Model	Area(m^2)	Reflection Rate (%)
Floor	21	20
Back Wall	9.45	55
Right Side Wall	16.2	55
Left Side Wall	16.2	55
Ceiling	21	85
Front Wall (Top)	0.7	55
Front Wall (Bottom)	3.15	55
Front Wall (Side)	1.28	55
Total	88.98	–
Average	–	55

Also, from the input values for the daylight illuminance prediction equation, the location index and penetration ratio of windows for verification points P1 to P5 for daylight illuminance value comparison were shown in Table 4.

Table 4. Illuminance sensor geometry and glazing transmittance of analysis model. (z = The horizontal distance between the window and sensor point (m), h_p = Height between lower edge of the window and sensor point (m), h_w = Window height (m), X_p = Distance between sensor point and left wall (m), X_w = Distance between the left edge of the window and left wall (m), W_w = Window width (m), τ_w = Visible light transmittance (%)).

Parameters	P1 (1 m)	P2 (2 m)	P3 (3 m)	P4 (4 m)	P5 (5 m)
Z	1	2	3	4	5
h_p	0.15	0.15	0.15	0.15	0.15
h_w	1.6	1.6	1.6	1.6	1.6
X_p	1.75	1.75	1.75	1.75	1.75
X_w	0.5	0.5	0.5	0.5	0.5
W_w	2.7	2.7	2.7	2.7	2.7
τ_w	78% (Visible Light Transmittance)				

3.2. Condition of Glazing and Shading Device to Evaluate Daylight Performance

Table 5 presents the set of simulation variables to evaluate daylight performance, by applying a simplified daylight prediction equation. To evaluate the visual environment the change of the sky model and the venetian blind slat angles can be adjusted. The façade orientation of the evaluation model was set to be facing south.

Table 5. Set of simulation variables for indoor illuminance.

Set of Simulation Variables for Indoor Illuminance (Façade Direction: South)		
Case 1–1	Double Clear (6CL+12A+6CL)/3.21 (Vernal equinox) at 07:00–18:00	CIE Overcast Sky
Case 1–2	Double Clear (6CL+12A+6CL)/6.21 (Summer solstice) at 07:00–18:00	
Case 1–3	Double Clear (6CL+12A+6CL)/9.21 (Autumnal equinox) at 07:00–18:00	
Case 1–4	Double Clear (6CL+12A+6CL)/12.21 (Winter solstice) at 07:00–18:00	
Case 2–1	Double Clear (6CL+12A+6CL)/3.21 (Vernal equinox) at 07:00–18:00	CIE Clear Sky
Case 2–2	Double Clear (6CL+12A+6CL)/6.21 (Summer solstice) at 07:00–18:00	
Case 2–3	Double Clear (6CL+12A+6CL)/9.21 (Autumnal equinox) at 07:00–18:00	
Case 2–4	Double Clear (6CL+12A+6CL)/12.21 (Winter solstice) at 07:00–18:00	
Case 3–1	Double Clear + Exterior Venetian Blind (Slat Angle: 30°)/3.21 (Vernal equinox) at 07:00–18:00	
Case 3–2	Double Clear + Exterior Venetian Blind (Slat Angle: 30°)/6.21 (Summer solstice) at 07:00–18:00	
Case 3–3	Double Clear + Exterior Venetian Blind (Slat Angle: 30°)/9.21 (Autumnal equinox) at 07:00–18:00	
Case 3–4	Double Clear + Exterior Venetian Blind (Slat Angle: 30°)/12.21 (Winter solstice) at 07:00–18:00	
Case 4–1	Double Clear + Exterior Venetian Blind (Slat Angle: 45°)/3.21 (Vernal equinox) at 07:00–18:00	
Case 4–2	Double Clear + Exterior Venetian Blind (Slat Angle: 45°)/6.21 (Summer solstice) at 07:00–18:00	
Case 4–3	Double Clear + Exterior Venetian Blind (Slat Angle: 45°)/9.21 (Autumnal equinox) at 07:00–18:00	
Case 4–4	Double Clear + Exterior Venetian Blind (Slat Angle: 45°)/12.21 (Winter solstice) at 07:00–18:00	
Case 5–1	Double Clear + Exterior Venetian Blind (Slat Angle: 60°)/3.21 (Vernal equinox) at 07:00–18:00	
Case 5–2	Double Clear + Exterior Venetian Blind (Slat Angle: 60°)/6.21 (Summer solstice) at 07:00–18:00	
Case 5–3	Double Clear + Exterior Venetian Blind (Slat Angle: 60°)/9.21 (Autumnal equinox) at 07:00–18:00	
Case 5–4	Double Clear + Exterior Venetian Blind (Slat Angle: 60°)/12.21 (Winter solstice) at 07:00–18:00	

Case 1–1 through 1–4 evaluated indoor daylight illuminance when double clear (6CL + 12A + 6CL) was installed with the CIE standard overcast sky for seasonal representative dates (21st March, 21st June, 21st September and 21st December). Case 2–1 through 2–4 evaluated indoor daylight illuminance when double clear (6CL + 12A + 6CL) was installed with the CIE standard clear sky. Cases 3 through 5 additionally installed exterior venetian blinds to change the angles from 30°–60°. The 21st of March, June, September and December were chosen as simulation dates to represent spring, summer, fall and winter, which were intended to be representative of the Sun's positioning during Korea's four seasons. The entire day, excluding the night time, 07:00–18:00 (12 h) was chosen as the simulation time to evaluate the effect of solar radiation input based on the Sun.

Characteristics of the venetian blind [60] were based on a commercially available product, and the blind's material properties and slat angle's setup were presented as shown Figure 7 and Table 6. Venetian blinds were installed on the exterior of the simulation model's windows, so the entire side can be controlled.

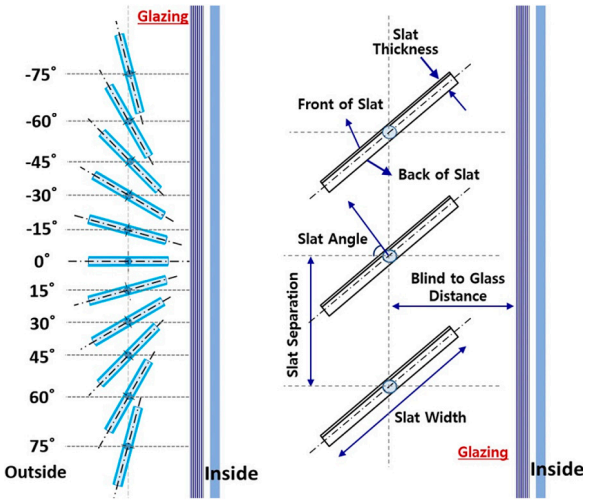

Figure 7. Properties of the venetian blind [60].

Table 6. Set of the venetian blind slat angle and dimensions.

Blind Conditions	Exterior Blind
Slat Width (mm), Slat Separation (mm)	50
Slat Thickness (mm)	2
Slat Conductivity (W/mk)	221
Slat Beam & Diffuse Solar Reflectance	0.7
Slat Infrared Emissivity	0.9
Blind to Glass Distance (mm)	25

4. Sky Luminance Distribution Results and Analysis

4.1. Sky Luminance Distribution

Figure 8 shows the sky patch that was used to calculate sky luminance of each location by dividing the sky into 145 elements [36]. As indicated previously, the applicable sky models included CIE standard overcast sky and CIE clear sky. To apply the sky luminance L value to the indoor illuminance prediction equation, algorithm framework of sky luminance distribution in Figure 3 were used to create sky luminance distribution (sky luminance/zenith luminance) of CIE overcast sky and clear sky.

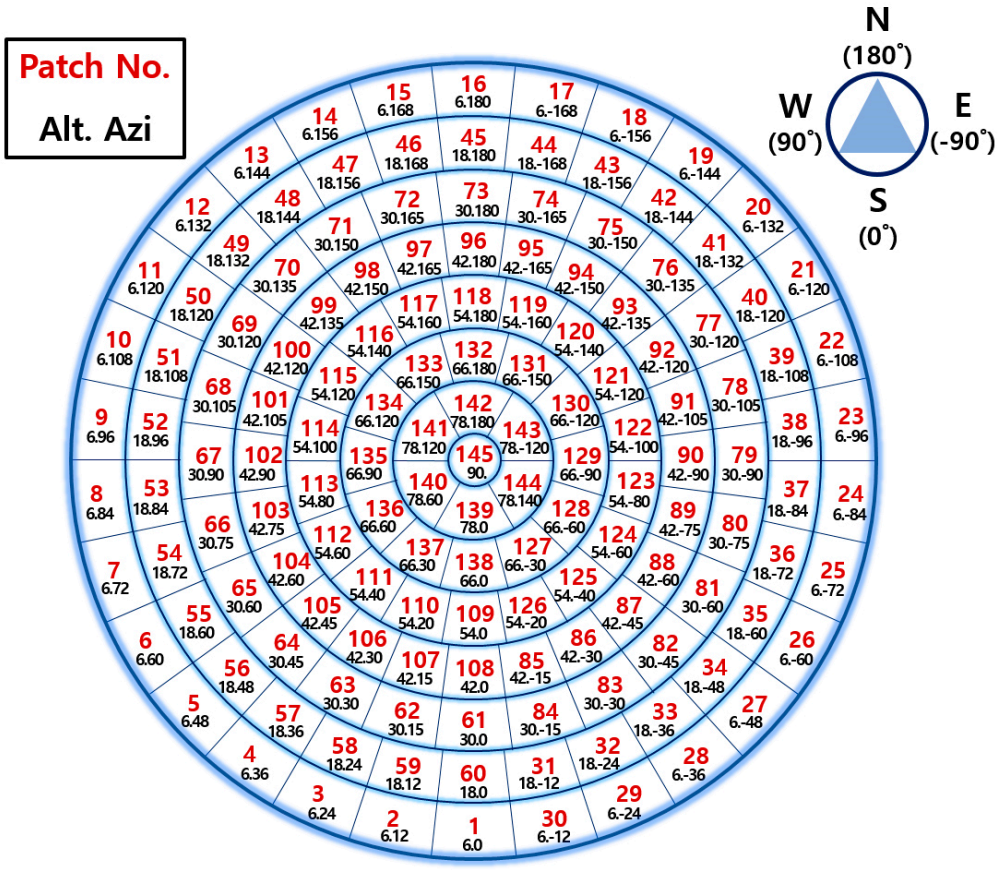

Figure 8. Calculation points for the sky patches.

Table 7 shows luminance distribution on the 21st of March, June, September, and December at 2:00 pm with an overcast sky. Sky luminance distribution ratio value was the same for seasonal representative dates. From the standard overcast sky on the 21st March, June, September, and December at 2:00 pm, the horizon/luminance ratio was approximately 3:1. When the CIE standard overcast sky's luminance distribution was employed, the ratio of the sky's relative luminance distribution to

zenith luminance ranged from 0.3 to 1, indicating that the zenith luminance was approximately 3 times brighter than the luminance near the horizon. Also, in overcast sky conditions, the luminance for all azimuths were identical when the elevation of the sky positions were identical. The CIE overcast sky's luminance distribution was at its highest near the zenith (Patch No. 145).

Table 7. Sky luminance distribution of CIE standard overcast sky.

Min: 0	Sky luminance distribution ratio = Sky luminance/Zenith luminance	Max: 1

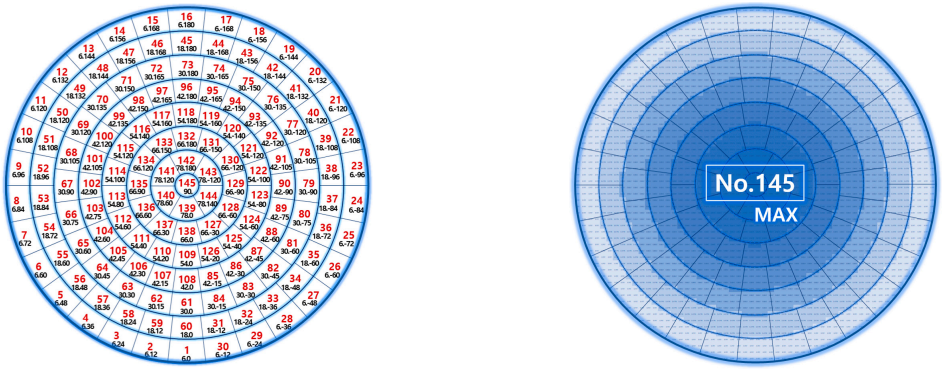

CIE Standard Overcast Sky_3.21 at 2:00 pm (Sun's Location: Altitude 48.03°, Azimuth 30.09°)
CIE Standard Overcast Sky_6.21 at 2:00 pm (Sun's Location: Altitude 67.07°, Azimuth 58.31°)
CIE Standard Overcast Sky_9.21 at 2:00 pm (Sun's Location: Altitude 46.53°, Azimuth 45.39°)
CIE Standard Overcast Sky_12.21 at 2:00 pm (Sun's Location: Altitude 25.68°, Azimuth 22.31°)

Table 8 shows luminance distribution on the 21st of March, June, September, and December at 2:00 pm in clear sky conditions. The sun's altitude was 48.03° using a standard clear sky on the 21st March at 2:00 pm. The azimuth was 30.09°, and Patch No.106's luminance value was highest where the sun was located. The opposite side of the sun around Patch No.119 gets low luminance distribution. This luminance value was approximately eight times higher than the ceiling luminance. Also, the distribution on 21st September was similar to that on 21st March. The patch No.105's luminance value was highest where the sun was located. However, on the opposite side of the sun at Patch No.120, the lowest luminance value was shown, and the surrounding distribution also showed the lowest value. The location of the sun's altitude was 67.07°, and the azimuth was 58.31° on 21st June at 2:00 pm. From Patch No.136 where the sun was located, a high luminance distribution and ceiling luminance got approximately five times more luminance, whereas the opposite side of the sun around Patch No. 130 got low luminance distribution. The sun's altitude was 25.68° on 21st December at 2:00 pm., and the luminance distribution was at its highest when the sun was located at Patch No. 58 and at its lowest at Patch No. 131.

Table 8. Sky luminance distribution of CIE standard clear sky.

Min: 0	Sky luminance distribution ratio = Sky luminance/Zenith luminance	Max: 14

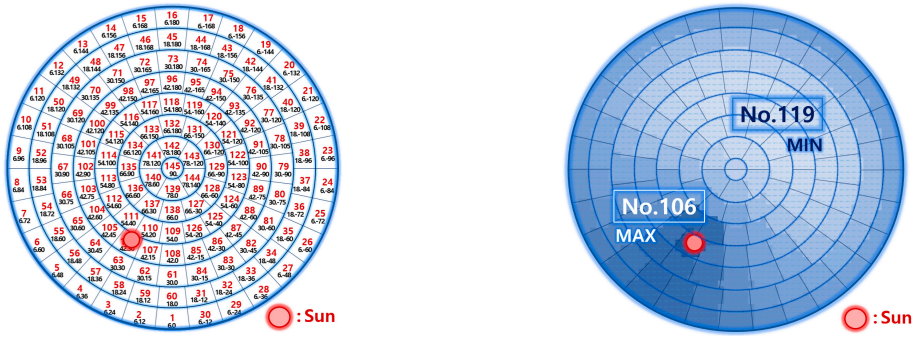

CIE Standard Clear Sky_3.21 at 2:00 pm (Sun's Location: Altitude 48.03°, Azimuth 30.09°)

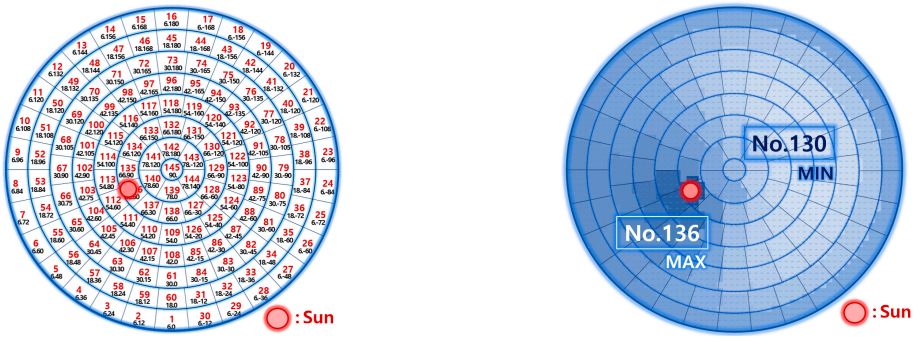

CIE Standard Clear Sky_6.21 at 2:00 pm (Sun's Location: Altitude 67.07°, Azimuth 58.31°)

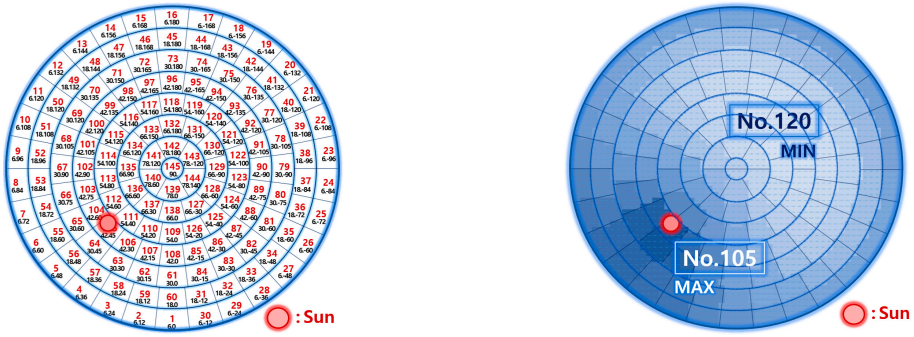

CIE Standard Clear Sky_9.21 at 2:00 pm (Sun's Location: Altitude 46.53°, Azimuth 45.39°)

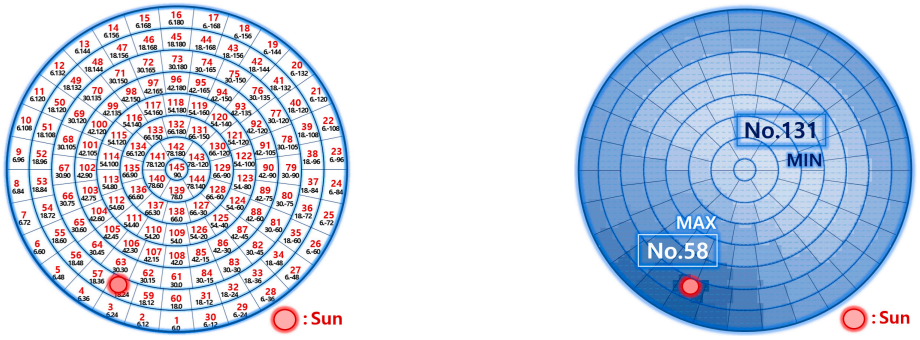

CIE Standard Clear Sky_12.21 at 2:00 pm (Sun's Location: Altitude 25.68°, Azimuth 22.31°)

4.2. Verification of Sky Luminance Distribution

We verified each patch of sky luminance value for the four directions (north, south, east and west) and for the seasonal representative dates (21st March, 21st June, 21st September, 21st December at 2pm) based on the position of the Sun instead of verifying the entire days' time, because we reviewed

and applied CIE general sky theories (in Figure 3). We verified each position of the Sun using the Sun's position of 2 pm where it is tilted towards the west from the southern direction. Figure 9 is a diagram depicting the sky element point's altitude and azimuth, which were compared with Desktop Radiance for verification, and the position of the Sun at each seasonal representative date (21st March, 21st June, 21st September, and 21st December) [61].

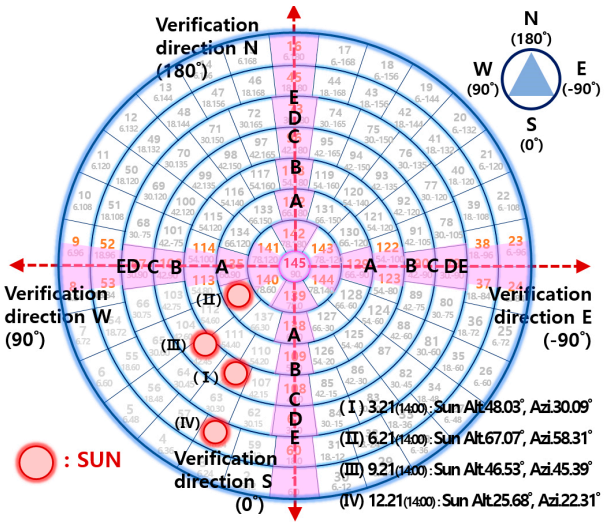

Figure 9. Verification points for the sky patches [61].

This study calculated the luminance of the four directions (North, South, East and West), and the calculation direction of each sky was −90°, 90°, 0°, and 180°. In other words, the verification of the Desktop Radiance program simulation value and sky luminance was conducted for the 20 positions represented by the four directions (azimuth) and the five sky calculation elevation positions (A, B, C, D, and E). Also, for CIE standard clear sky luminance distribution, the Sun's altitude and azimuth both serve as important variables, altering the distribution. Thus, the changes in the Sun's position (altitude, azimuth) on the seasonal representative dates were also considered.

Table 9 shows interior images of Desktop Radiance, concept diagram, and sky luminance (luminance value at the center of the window) location from each sensor. Window luminance values were different depending on the calculation location because the sensor gets the light through the window from different angles. Sky luminance is the center part of the sky visible to the point sensor through the window. The center of the window luminance was calculated using this concept. Since, sky luminance values are dependent on the sky condition, the center of window luminance in two sky models were calculated using Equations (1), (2), and (4).

It is important to find a location of sky patch to calculate illuminance. It is possible to find an angle looks at the sky from the sensor using a trigonometric function when the height of the window and horizontal distance are known. The location in simulation model is in Incheon, Korea (Latitude: 37.48°, Longitude: 126.55°), and the facade orientation is facing South. The sky location was at position A of the sky patch when looking at the sky from the illuminance sensor at 1 m the altitude was 61.6°, and since there is a window on the south side, the azimuth was 0°. When looking at the sky location of spot B–2 m from the illuminance sensor, the altitude was 42.8°. At 3 m, the sky location of spot C's altitude was 31.7°. At 4 m, spot D's altitude was 24.8°, and for 5 m, spot E's altitude was 20.3°, and since the azimuth's direction is south, the angle was 0°.

Table 9. Image of Desktop Radiance, concept diagram, and sky luminance from looking at each sensor.

Sensor	Sky Element's Location (South)	Sky Luminance (cd/m²)	
		Overcast Sky	Clear Sky
1 m (A)	Alt. 61.6° –Azi. 0°	2936 cd/m²	5197 cd/m²
2 m (B)	Alt. 42.8° –Azi. 0°	2516 cd/m²	6414 cd/m²
3 m (C)	Alt. 31.7° –Azi. 0°	2185 cd/m²	6146 cd/m²
4 m (D)	Alt. 24.8° –Azi. 0°	1946 cd/m²	6027 cd/m²
5 m (E)	Alt. 20.3° –Azi. 0°	1814 cd/m²	6070 cd/m²

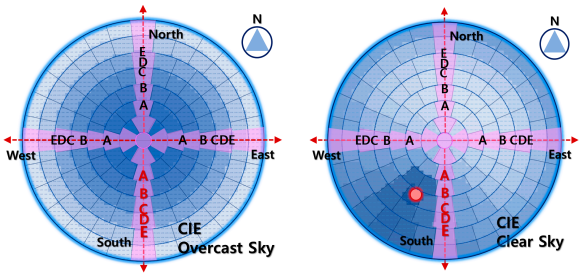

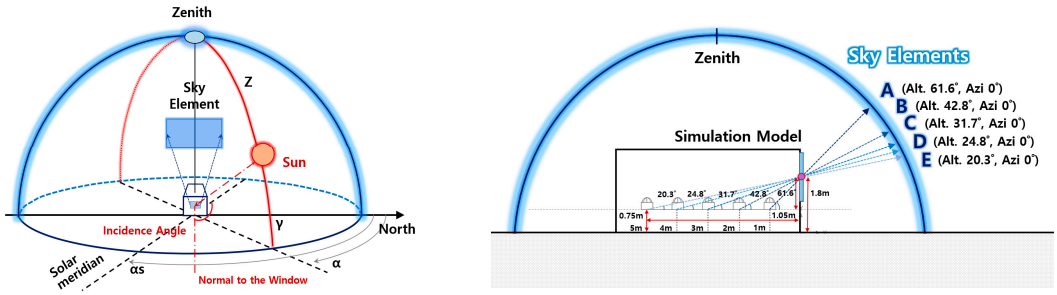

Concept of sky luminance where looking at the sky from the illuminance sensor (1–5 m), 3.21 at 2:00 pm, Direction: South

Sky luminance image of Radiance (The center of the part of the overcast sky visible to the point P through the window)

Sky luminance image of radiance (the center of the part of the clear sky visible to the point P through the window)

For clear sky conditions, sky luminance at spot A was 5197 cd/m^2, spot B was 6414 cd/m^2, spot C was 6146 cd/m^2, spot D was 6027 cd/m^2, and spot E was 6070 cd/m^2. On the other hand, a gradually decreasing tendency in sky luminance from spot A to E was observed in overcast sky conditions. Luminance was 2936 cd/m^2 at spot A, 2516 cd/m^2 at spot B, 2185 cd/m^2 at spot C, 1946 cd/m^2 at spot D, and 1814 cd/m^2 at spot E. These luminance values were applied to the modified version of predicted equation, and result of indoor illuminance by different sky models using the modified equation is presented in Section 5.

Verification of Sky Luminance Distribution for Overcast and Clear Sky

Table 10 shows the results of a comparison between sky luminance calculation value (CIE general sky theories in Figure 3) at 5 sky calculation elevation angles for overcast sky (A, B, C, D, and E) and the Desktop Radiance simulation value.

For 21st March, 21st June, 21st September, and 21st December at 2:00 pm of the overcast sky, the luminance values were the same for all four directions (North, South, East and West) when the sky

position's elevation was the same. Thus, the sky luminance value for the five positions (A, B, C, D, and E) in the four directions was also the same. When the sky luminance of 21st March results derived from the CIE general sky theories were compared with the Desktop Radiance simulation value, the luminance error rates for positions A, B, C, D, and E in four directions were 1.4%, 1.2%, 1.2%, 1.0%, and 0.5%, respectively. Comparison results of the 21st March, 21st June, 21st September and 21st December at 2:00 pm also showed error rates ranging between 0.5–1.6%, in all four directions.

Table 10. Prediction results and error rate of sky luminance distributions in CIE overcast sky.

3.21 at 2:00 pm (Sun Alt.48.03° Azi.30.09°)		**A–1 m(61.6°)**	**B–2 m(42.8°)**	**C–3 m(31.7°)**	**D–4 m(24.8°)**	**E–5 m(20.3°)**
Verification Direction (N,S,E, and W)	Desktop Radiance (cd/m^2)	2936	2516	2185	1964	1814
	Calculation (cd/m^2)	2978	2546	2212	1986	1825
	Error Rate (%)	1.4%	1.2%	1.2%	1.0%	0.5%
6.21 at 2:00 pm (Sun Alt.67.07° Azi.58.31°)		**A–1 m(61.6°)**	**B–2 m(42.8°)**	**C–3 m(31.7°)**	**D–4 m(24.8°)**	**E–5 m(20.3°)**
Verification Direction (N,S,E, and W)	Desktop Radiance (cd/m^2)	3620	3096	2705	2423	2241
	Calculation (cd/m^2)	3674	3137	2736	2445	2250
	Error Rate (%)	1.5%	1.3%	1.1%	0.9%	0.4%
9.21 at 2:00 pm (Sun Alt.46.53° Azi.45.39°)		**A–1 m(61.6°)**	**B–2 m(42.8°)**	**C–3 m(31.7°)**	**D–4 m(24.8°)**	**E–5 m(20.3°)**
Verification Direction (N,S,E, and W)	Desktop Radiance (cd/m^2)	2902	2477	2163	1933	1789
	Calculation (cd/m^2)	2941	2508	2187	1953	1799
	Error Rate (%)	1.3%	1.2%	1.1%	1.0%	0.5%
12.21 at 2:00 pm (Sun Alt.25.68° Azi.22.31°)		**A–1 m(61.6°)**	**B–2 m(42.8°)**	**C–3 m(31.7°)**	**D–4 m(24.8°)**	**E–5 m(20.3°)**
Verification Direction (N,S,E, and W)	Desktop Radiance (cd/m^2)	1724	1475	1288	1130	997
	Calculation (cd/m^2)	1753	1496	1305	1143	1007
	Error Rate (%)	1.6%	1.4%	1.3%	1.1%	0.9%

Table 11 shows the results of a comparison between sky luminance at five sky calculation elevation angles for clear sky positions (A, B, C, D, and E) and the simulation value. For 21st March at 2:00 pm, when the window was facing south, the sky luminance ranged from 5269 cd/m^2 to 6509 cd/m^2 due to its close proximity with the sun, and the sky luminance value was relatively high compared to other directions. When the luminance result derived using the CIE sky algorithm was compared with the Desktop Radiance simulation value, the luminance error rates from positions A through E ranged from 0.8% to 1.4%, respectively. When the window was facing west, sky luminance values ranged from 3225 to 3730 cd/m^2, and the error rates between the calculated value and the Desktop Radiance simulation value ranged from 0.9% to 1.5%, respectively. When the window was facing east, sky luminance values range from 1687 to 2278 cd/m^2, and the error rates between the calculated value and the simulation value ranged from 0.6% to 1.4%, respectively. When the window was facing north, sky luminance values ranged from 1475 to 2271 cd/m^2, and the error rates between the calculated value and the simulation value ranged from 0.7% to 1.3%, respectively. Comparison results of the 21st March, 21st June, 21st September and 21st December at 2:00 pm also showed error rates ranging from 0.4% to 1.6%, in each direction.

Table 11. Prediction results and error rate of sky luminance distributions in CIE clear sky.

3.21 at 2:00 pm (Sun Alt.48.03° Azi.30.09°)		**A–1 m(61.6°)**	**B–2 m(42.8°)**	**C–3 m(31.7°)**	**D–4 m(24.8°)**	**E–5 m(20.3°)**
Verification	Desktop Radiance (cd/m^2)	1460	1459	1500	1971	2241
Direction	Calculation (cd/m^2)	1475	1478	1519	1998	2271
(North)	Error Rate (%)	0.9%	1.2%	1.3%	1.3%	1.0%
Verification	Desktop Radiance (cd/m^2)	5197	6414	6146	6027	6070
Direction	Calculation (cd/m^2)	5269	6509	6236	6105	6123
(South)	Error Rate (%)	1.0%	1.0%	1.4%	1.0%	0.8%
Verification	Desktop Radiance (cd/m^2)	1663	1623	1802	2031	2265
Direction	Calculation (cd/m^2)	1687	1636	1814	2048	2278
(East)	Error Rate (%)	1.4%	0.8%	0.7%	0.8%	0.6%
Verification	Desktop Radiance (cd/m^2)	3184	3281	3350	3507	3694
Direction	Calculation (cd/m^2)	3225	3329	3403	3555	3730
(West)	Error Rate (%)	1.0%	1.0%	1.5%	1.3%	0.9%
6.21 at 2:00 pm (Sun Alt.67.07° Azi.58.31°)		**A–1 m(61.6°)**	**B–2 m(42.8°)**	**C–3 m(31.7°)**	**D–4 m(24.8°)**	**E–5 m(20.3°)**
Verification	Desktop Radiance (cd/m^2)	1127	953	1002	1103	1214
Direction	Calculation (cd/m^2)	1145	962	1008	1110	1220
(East)	Error Rate (%)	1.5%	0.8%	0.5%	0.6%	0.4%
Verification	Desktop Radiance (cd/m^2)	3645	2531	2184	2124	2141
Direction	Calculation (cd/m^2)	3693	2555	2217	2151	2172
(West)	Error Rate (%)	1.1%	0.9%	1.4%	1.2%	1.0%
Verification	Desktop Radiance (cd/m^2)	2436	1847	1729	1725	1784
Direction	Calculation (cd/m^2)	2467	1875	1732	1742	1798
(South)	Error Rate (%)	1.2%	1.1%	1.3%	0.9%	0.7%
Verification	Desktop Radiance (cd/m^2)	1281	1054	1081	1163	1265
Direction	Calculation (cd/m^2)	1300	1069	1091	1178	1277
(North)	Error Rate (%)	1.0%	1.3%	0.8%	1.2%	0.9%
9.21 at 2:00 pm (Sun Alt.46.53° Azi.45.39°)		**A–1 m(61.6°)**	**B–2 m(42.8°)**	**C–3 m(31.7°)**	**D–4 m(24.8°)**	**E–5 m(20.3°)**
Verification	Desktop Radiance (cd/m^2)	1561	1566	1794	2072	2344
Direction	Calculation (cd/m^2)	1583	1580	1808	2086	2354
(East)	Error Rate (%)	1.3%	0.8%	0.7%	0.6%	0.4%
Verification	Desktop Radiance (cd/m^2)	4105	4696	4742	4849	5015
Direction	Calculation (cd/m^2)	4144	4741	4802	4911	5063
(West)	Error Rate (%)	0.9%	0.9%	1.2%	1.2%	0.9%
Verification	Desktop Radiance (cd/m^2)	4052	4588	4650	4766	4946
Direction	Calculation (cd/m^2)	4091	4657	4723	4837	4993
(South)	Error Rate (%)	0.9%	1.1%	1.5%	1.4%	0.9%
Verification	Desktop Radiance (cd/m^2)	1574	1562	1784	2066	2335
Direction	Calculation (cd/m^2)	1588	1584	1810	2087	2354
(North)	Error Rate (%)	0.8%	1.1%	1.0%	0.9%	0.8%
12.21 at 2:00 pm (Sun Alt.25.68° Azi.22.31°)		**A–1 m(61.6°)**	**B–2 m(42.8°)**	**C–3 m(31.7°)**	**D–4 m(24.8°)**	**E–5 m(20.3°)**
Verification	Desktop Radiance (cd/m^2)	2152	2442	2877	3079	3505
Direction	Calculation (cd/m^2)	2188	2470	2919	3122	3545
(East)	Error Rate (%)	1.6%	1.1%	1.0%	1.4%	1.1%
Verification	Desktop Radiance (cd/m^2)	3025	3733	4349	4921	5418
Direction	Calculation (cd/m^2)	3063	3781	4418	4988	5480
(West)	Error Rate (%)	1.2%	1.0%	1.5%	1.3%	1.1%
Verification	Desktop Radiance (cd/m^2)	4854	5560	6847	7414	8842
Direction	Calculation (cd/m^2)	4916	5625	6940	7499	8944
(South)	Error Rate (%)	1.2%	1.2%	1.4%	1.1%	1.2%
Verification	Desktop Radiance (cd/m^2)	1948	2377	3024	3675	4261
Direction	Calculation (cd/m^2)	1971	2412	3062	3717	4306
(North)	Error Rate (%)	1.1%	1.4%	1.2%	1.1%	1.0%

Based on the data given in Tables 10 and 11, Figure 10 shows the Pearson correlation coefficient R^2 [62], MBE [63], RMSE [63], Cv(RMSE) [63] analysis and *t*-test (*t*-value, *p*-value) [64] results of Desktop Radiance simulation and the CIE general sky theories calculation on the two sky types with four seasonal representative dates (21st March, 21st June, 21st September, and 21st December), four directions (North, South, East and West) on five locations (A–E). The luminance distribution was 997–3674 cd/m^2 for an overcast sky and 953–8944 cd/m^2 for a clear sky. For both types of sky models, the luminance value of the simulation and the calculated result of equation had a Pearson correlation coefficient R^2 over 0.99, MBE value less than ±10%, and Cv (RMSE) value less than 30%, showing a high correlation satisfying the American Society of Heating, Refrigerating and Air–Conditioning Engineers (ASHRAE) guidelines [63]. The *t*-test results with a significance level of 0.05 showed a *p*-value less than 0.05. Therefore, the calculation results from the algorithm framework of CIE sky luminance distribution have a statistical significance with the Desktop Radiance Simulation results.

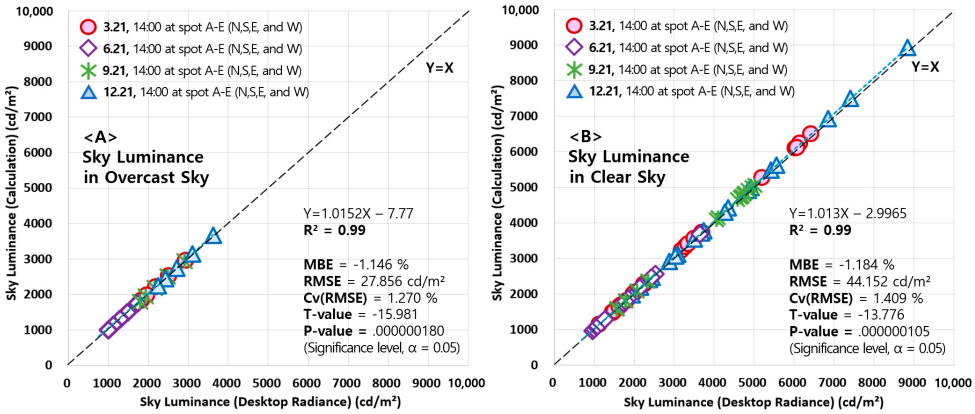

Figure 10. Comparison of sky luminance between the CIE sky algorithm and Desktop Radiance. (**A**) Overcast sky (**B**) Clear sky.

5. Evaluation of Indoor Illuminance

5.1. Verification on Indoor Illuminance Prediction Method (CIE Overcast Sky)

Figure 11 shows the results of a comparison between the Desktop Radiance simulation result and modified equations for overcast sky conditions. Indoor illuminance distribution results for the 21st of March, June, September, and December at 2:00 pm are presented. The illuminance prediction error rate was 1%–9% from 1 to 5 m when predicting illuminance using the modified equation on 21st March. At 1 m, the error rate was 5% when comparing result of indoor illuminance using the modified equation and result of the Desktop Radiance simulation. At 2 m, the error rate was 8%. At 3 m, the error rate was 9% when comparing results of indoor illuminance using the modified equation and result of the simulation. Also, at 4 m and 5 m, illuminance prediction error rate of the modified equation ranged from 1% to 3%, prediction of illuminance using modified equation was accurate compare with the Desktop Radiance results. The illuminance prediction error rate was 2%–7% from 1 to 5 m when predicting illuminance using the modified equation on 21st June. The average error rate of illuminance prediction was 5.1%. The average error rate of illuminance prediction was 5.5% on 21st September, and the illuminance prediction error rate ranged from 2% to 8% from 1 to 5 m when predicting illuminance using the modified equation on 21st September. Finally, on 21st December, the average error rate of illuminance prediction was 6.7%.

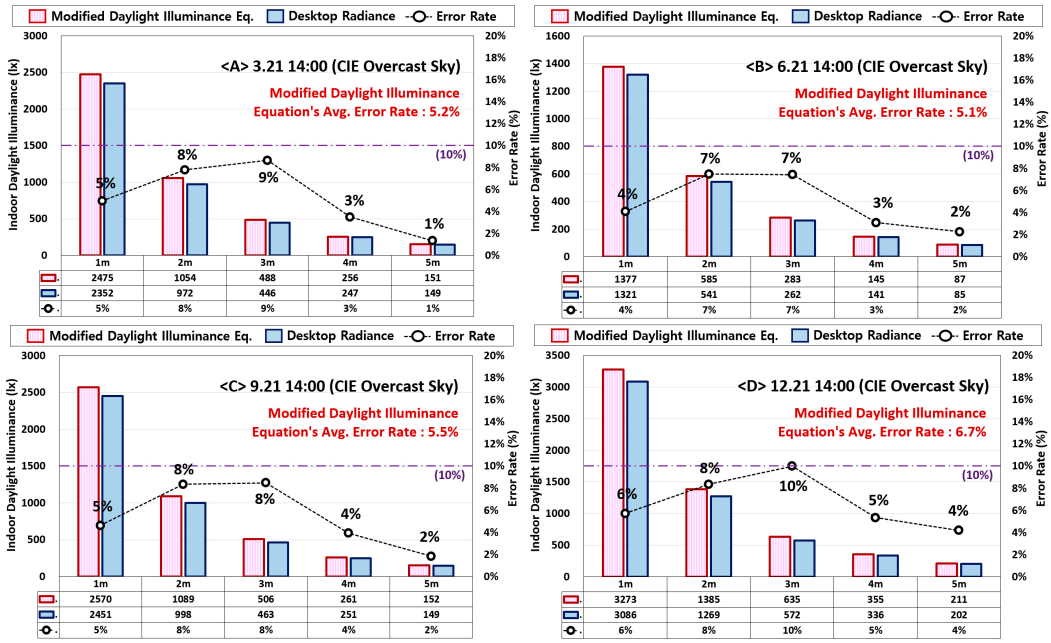

Figure 11. Comparison of indoor daylight illuminance between the modified equation and Desktop Radiance in CIE overcast sky condition (**A**) 3.21, 14:00 (**B**) 6.21, 14:00 (**C**) 9.21, 14:00 (**D**) 12.21, 14:00.

While Figure 11 shows detailed results at a specified time (14:00) on 21st March, 21st June, 21st September and 21st December, Figure 12 shows the results of a comparison between the Desktop Radiance simulation result and a modified equations result in overcast sky for the entire day, excluding the night time, 07:00–18:00 (12 h).

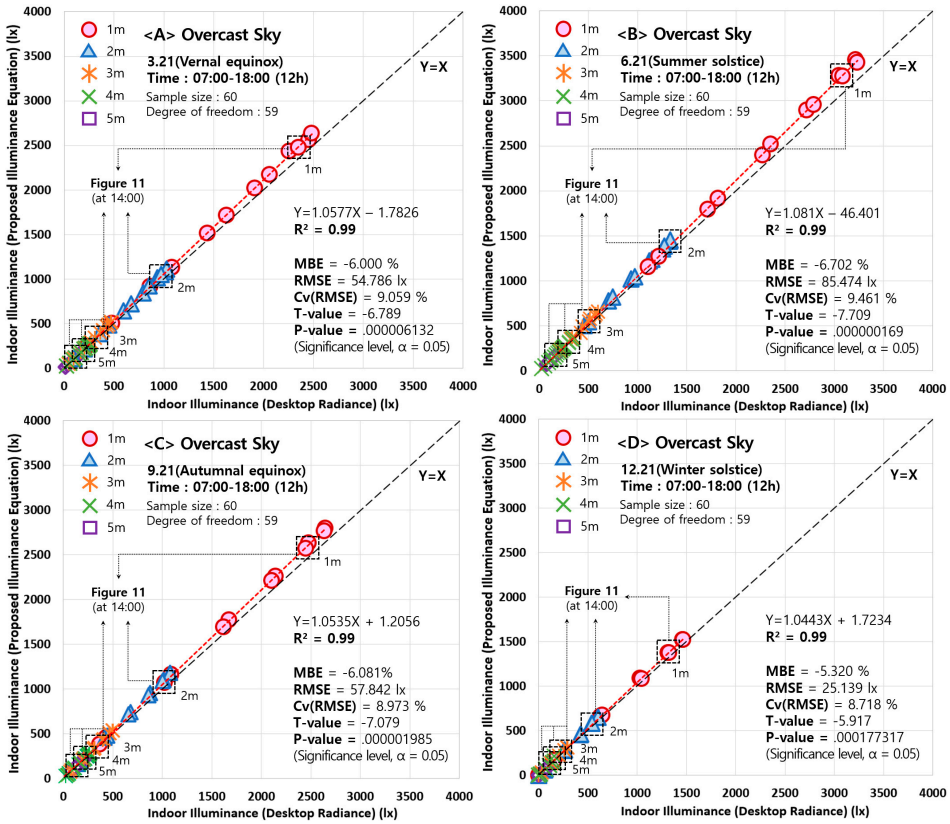

Figure 12. Comparison of indoor illuminance between the modified equation and Desktop Radiance in CIE overcast sky (**A**) 3.21 (**B**) 6.21 (**C**) 9.21 (07:00–18:00) (**D**) 12.21 (07:00–18:00).

The R^2, MBE, RMSE, Cv (RMSE) analysis and *t*-test (*t*-value, *p*-value) was done on the simulation results of each illuminance sensor (1 m–5 m) at 07:00–18:00 (12 h, all day excluding the night time) and the calculation results of the proposed equation. In case of an overcast sky, the illuminance was distributed between 0–3000 lx for 21st March and 21st September, 0–3500 lx for 21st June and 0–1500 lx for 21st December. For the overcast sky illuminance, it was the highest at the summer solstice (6.21) and the lowest at the winter solstice (12.21).

The Desktop Radiance simulation results and the proposed equation calculation results of the four seasonal representative dates showed high correlations, all having a Pearson correlation coefficient R^2 value over 0.99, MBE value less than ±10% and Cv(RMSE) value less than 30%. The *t*-test results with a significance level of 0.05 showed a *p*-value of less than 0.05. Therefore the Desktop Radiance simulation result and proposed daylight equation calculation results were shown to have statistical significance. Tables S1-1, S1-2, S1-3, and S1-4 in the supplementary material provide the detailed data for 21st March, 21st June, 21st September, and 21st December at 07:00–18:00 for Figure 12.

Figure 13 shows the comparison between exterior horizontal illuminance and the daylight factor of each seasonal representative dates (overcast sky) using the proposed equation and the Desktop Radiance simulation. Furthermore, the DF values were compared and divided into their SC and IRC.

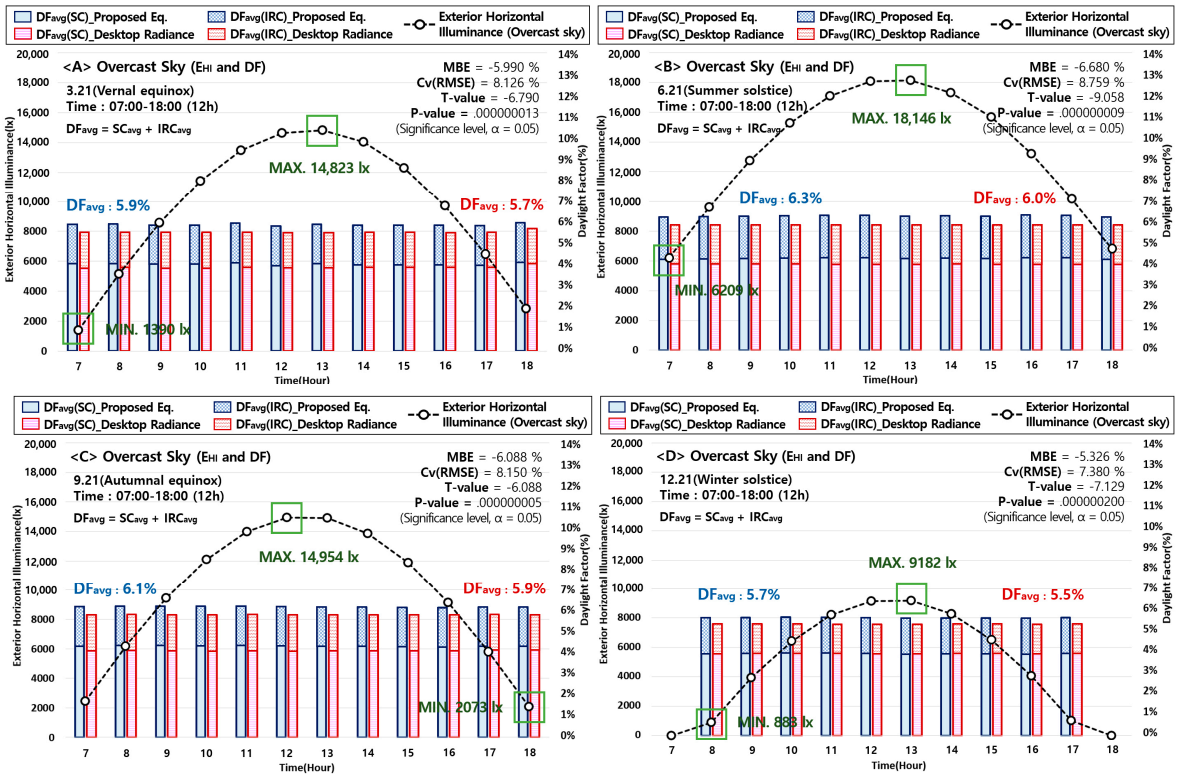

Figure 13. Comparison of daylight factor between the modified equation and Desktop Radiance simulation in CIE overcast sky (**A**) 3.21 (**B**) 6.21 (**C**) 9.21 (**D**) 12.21 (07:00–18:00).

The illuminance from natural sources is often determined in terms of the DF, which is the ratio of the indoor illuminance to the outdoor illuminance available on a horizontal plane from the entire overcast sky and is expressed as a percentage. The daylight factor is internationally recognized as the synthetic parameter to relate indoor visual task lighting requirements and daylight availability. From an energy perspective, it is also used in the new daylighting European Standard EN–17037:2018 [65] for evaluating daylight penetration of buildings. Standard sky for DF calculation (overcast sky) has been defined as the most conservative, and from an energy point of view, this is very useful since it represents the condition of peak energy consumption for artificial lighting [65–68].

Comparing the exterior horizontal illuminance of each seasonal representative dates (overcast sky), the exterior horizontal illuminance of 6.21 (07:00–18:00) was the highest, showing a distribution from 6209 lx to 18,146 lx. The exterior horizontal illuminance of 12.21 (07:00–18:00) was the lowest, showing a distribution from 883lx to 9218 lx. Unlike the case with exterior horizontal illuminance distribution, the four representative dates for an overcast sky had relatively constant DF values between 07:00–18:00, respectively. The calculations from the proposed equation showed that the average DF of 3.21, 6.21, 9.21, and 12.21 were 5.9, 6.3, 6.1, and 5.7%, respectively.

After dividing the results into SC and IRC components, the Desktop Radiance simulation value and statistical analysis were done. They showed a high correlation with MBE and Cv(RMSE) values satisfying the ASHRAE standards (MBE less than ±10%, Cv(RMSE) less than 30%) [63]. The *t*-test result with a significant level of 0.05 showed a *p*-value less than 0.05. Therefore, the DF (SC+IRC) value calculated from the equation proposed in this study have statistical significance with the Desktop Radiance simulation results. We also checked the average DF value compared with the DF of Mangione et al. [66] for the validity of calculated DF value using the proposed prediction method. The calculated DF value was found to be similar to the DF value of Mangione's study [66]. Tables S2-1, S2-2, S2-3, and S2-4 in the Supplementary Material provide detailed data for 21st March, 21st June, 21st September, and 21st December at 07:00–18:00 for Figure 13.

5.2. Verification on Indoor Illuminance Prediction Method (CIE Clear Sky)

When predicting illuminance for CIE clear sky condition, it is important that solar radiation influxes into the building. For this reason, the simulation model was unfolded into six sides, and indoor illuminance distribution was evaluated. Red represented a relatively high illuminance value, yellow was the median value, and green represented relatively low illuminance.

Figure 14 shows a comparison of the indoor illuminance using the modified equation and the Desktop Radiance simulation on 21st March at 2:00 pm (CIE clear sky). At 2:00 pm on 21st March, the sun was located near Patch No. 106. Therefore, it was possible to see some solar radiation input on the right wall of the six–sided planar figure. The lower depth shows lower luminance. At the illuminance sensor on 21st March at 2:00 pm from 1 to 5 m, the illuminance sensor was not affected by direct sunlight. Thereafter, the equations that consider the influence of diffuse and reflected illuminance were used in the formation of a prediction method.

When comparing Desktop Radiance simulation results at measurement point from 1 to 5 m, the proposed prediction equation's error rate ranged from 2% to 8%, and the overall average error rate was 4.9%. When analyzing the illuminance prediction error rate by distance, the error rate was 8% at 1 m and 6% at 2 m and 3 m. The error rate was 2%–3% at 4 m and 5 m, which is similar to the Desktop Radiance simulation values. The modified equation showed an overall tendency to express higher values than the Desktop Radiance simulation results. As the position of the illuminance sensor changes from 1 m to 5 m, the error rate of illuminance tends to decrease.

Figure 15 shows a comparison graph of indoor illuminance values that were calculated using the proposed prediction equation and the Desktop Radiance simulation on 21st June at 2:00 pm when the sun was located near Patch No. 136.

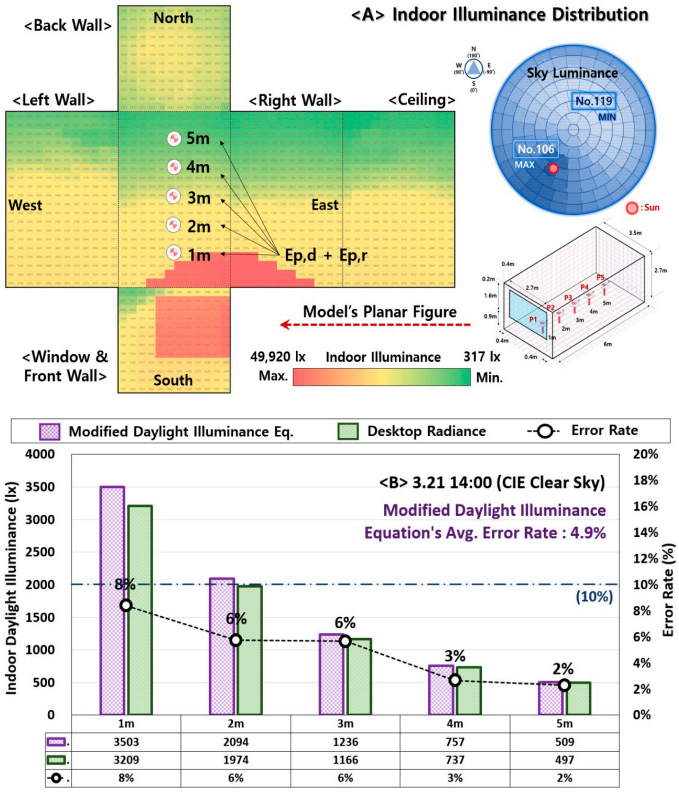

Figure 14. Indoor illuminance distribution of the six–side planar figure and comparison of illuminance between the modified equation and Desktop Radiance (CIE Clear Sky_3.21 14:00).

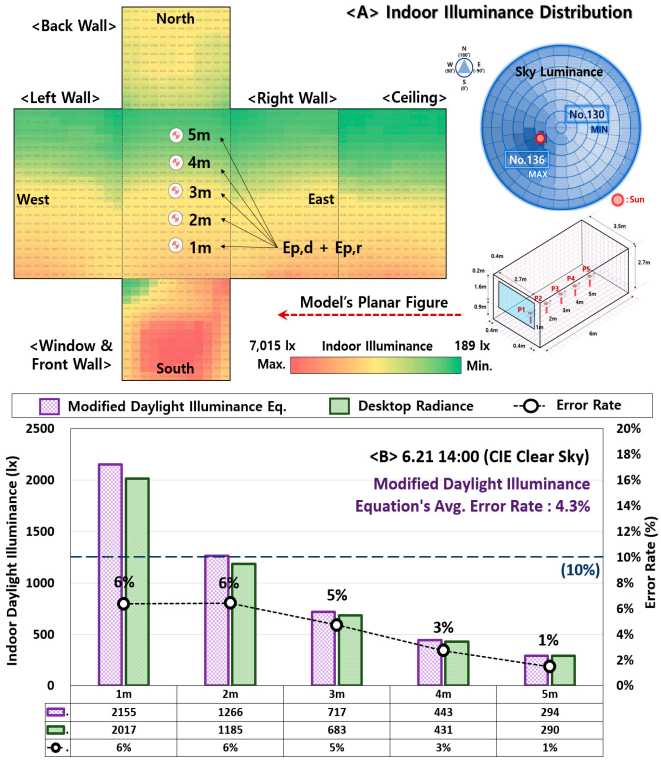

Figure 15. Indoor illuminance distribution of the six–side planar figure and comparison of illuminance between the modified equation and Desktop Radiance (CIE Clear Sky_6.21 14:00).

Since the sun's altitude was high that day at 2:00 pm, which represented a typical summer day (summer solstice), there was no direct sunlight effect at measurement point from 1 to 5 m. When comparing Desktop Radiance simulation result at measurement points of 1–5 m, the error rate ranged from 1% to 6%, and the overall average error rate was 4.3%. When analyzing the illuminance prediction error rate by distance, the error rate was 6% at 1 m, 6% at 2 m, 5% at 3 m, 3% at 4 m, and 1% at 5 m.

Figure 16 shows the indoor illuminance prediction results on 21st September at 2:00 pm when the sun was located near Patch No. 105. Direct solar radiation entered deeply into the building. The solar radiation input on the floor and the right wall of the six–sided planar figure are visible. For this reason, there was a direct sunlight effect at the measurement point at 1 m. Therefore, the influence from the direct solar beam was considered, and Equation (12)'s incidence angle was added. When comparing Desktop Radiance simulation result at measurement points of 1–5 m, the overall average error rate was 5.4%. The error rate was 7% at 1 m, 7% at 2 m, 6% at 3 m, 3% at 4 m, and 3% at 5 m.

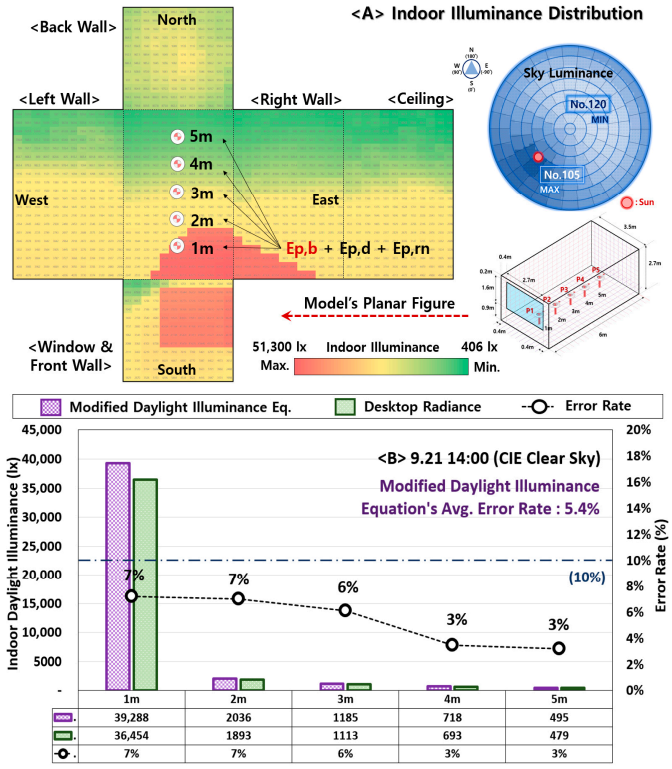

Figure 16. Indoor illuminance distribution of the six–side planar figure and comparison of illuminance between the modified equation and Desktop Radiance (CIE Clear Sky_9.21 14:00).

Figure 17 shows the indoor illuminance prediction results on 21st December at 2:00 pm, which represented a typical winter day (winter solstice), and the sun was located near Patch No. 58. Since the sun's altitude was low, direct solar radiation entered more deeply into the building. The solar radiation input on the floor and the right wall of the six–sided planar figure are visible. For this reason, there was a direct sunlight effect at the measurement point at 1 m. Therefore, the influence from the direct solar beam was considered, and Equation (12)'s incidence angle was added. When comparing Desktop Radiance simulation result at the measurement point of 1–5 m, the error rate ranged from 3% to 9%, and overall average error rate was 6.1%. When the modified prediction equation was used for winter solstice conditions, the effect of sky luminance, direct solar radiation, and indoor reflective components were reflected.

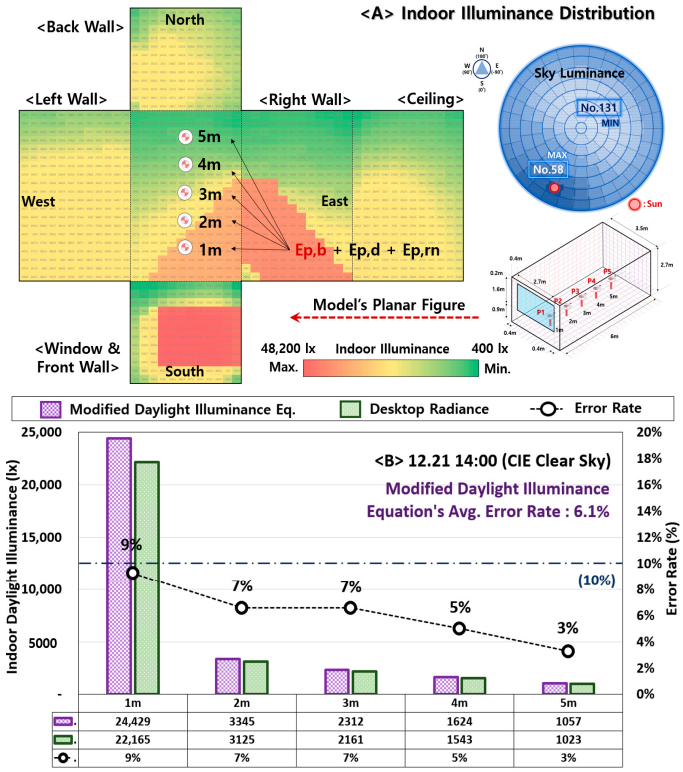

Figure 17. Indoor illuminance distribution of the six–side planar figure and comparison of illuminance between the modified equation and Desktop Radiance (CIE Clear Sky_12.21 14:00).

While Figures 14–17 shows detailed results at a specified time (14:00) on 21st March, 21st June, 21st September and 21st December, Figure 18 shows the result of a comparison between the Desktop Radiance simulation result and modified equations result in clear sky conditions for the entire day, excluding the night time, 07:00–18:00 (12 h).

The R^2, MBE, RMSE, Cv (RMSE) analysis and *t*-test (*t*-value, *p*-value) was done on the Desktop Radiance simulation results of each illuminance sensor (1 m–5 m) at 07:00–18:00 (12 h, all day excluding the night time) and the calculation results of the proposed equation.

The indoor illuminance of the clear sky was higher than that of the overcast sky, due to the influence of direct solar radiance. The indoor illuminance of a clear sky was distributed between 0–4500 lx for 21st of March and 21st of September, 0–2700 lx for 12.21 and 0–2500 lx for the 21st of June. For clear sky illuminance, it was the highest at the representative dates of the intermediate seasons (21st March & 21st September) and the lowest at the winter solstice (21st December). All four seasonal representative dates showed Desktop Radiance simulation and proposed equation calculation results' Pearson correlation coefficient R^2 equal to or higher than 0.99. The MBE and Cv (RMSE) values were less than ±10%, 30%, respectively. The MBE and Cv (RMSE) value satisfied the ASHRAE standard [63]. The *t*-test result with Significance level set to 0.05 showed that the *p*-value was also less than the significance level of 0.05. Thus, in comparison to Desktop Radiance simulation value, proposed daylight equation's calculation results possess statistical significance and were considered to be similar. Tables S3-1, S3-2, S3-3, and S3-4 in the Supplementary Material provide detailed data for 21st March, 21st June, 21st September, and 21st December at 07:00–18:00 for Figure 18.

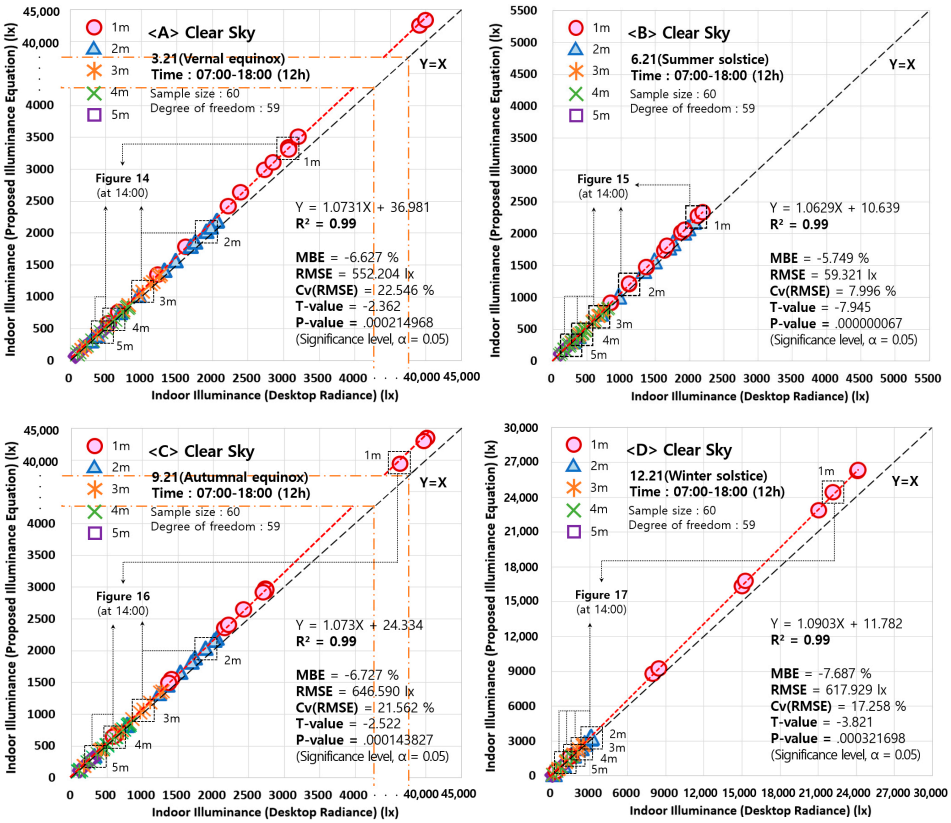

Figure 18. Comparison of indoor illuminance between the modified equation and Desktop Radiance in CIE clear sky (**A**) 3.21(07:00–18:00) (**B**) 6.21(07:00–18:00) (**C**) 9.21(07:00–18:00) (**D**) 12.21 (07:00–18:00).

5.3. Verification on Indoor Illuminance Prediction Method When Installing Venetian Blind (CIE Clear Sky)

Lastly, the possibility of predicting illuminance by applying the modified equation when installing the venetian blind under clear sky conditions was verified. To do this, the blind slat angle was set as a variable and the Desktop Radiance simulation results were compared with the modified equation results. Visible light transmittance of blinds can be calculated using LBNL's Window 7.6 program [69], as shown in Figure 19. It is possible to predict indoor illuminance by substituting the visible light transmittance (VLT) value of glass or blind in the modified equation.

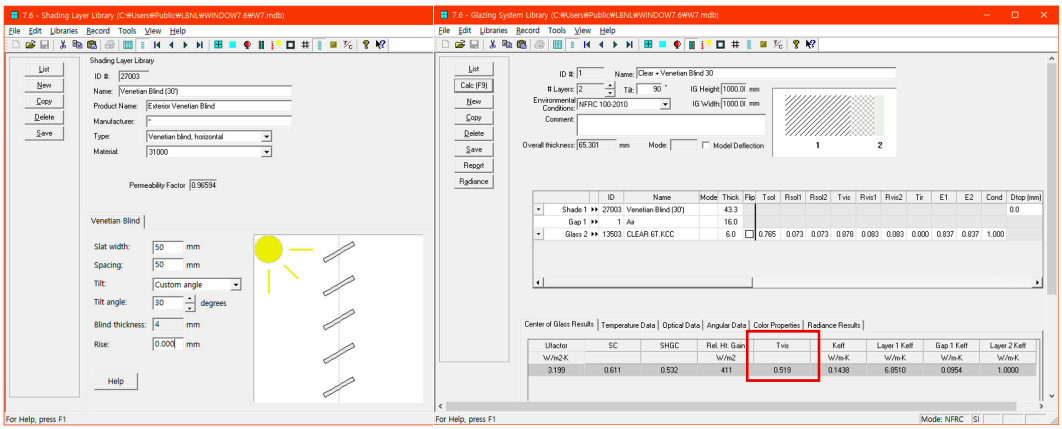

Figure 19. Calculation of visible light transmittance of blind using LBNL's Window 7.6 program.

Figure 20 is a graph that compares the results of Desktop Radiance and the proposed prediction method when installing external venetian blinds at an angle of 30° on 21st March, 21st June, 21st September, and 21st December at 2:00 pm (CIE clear sky).

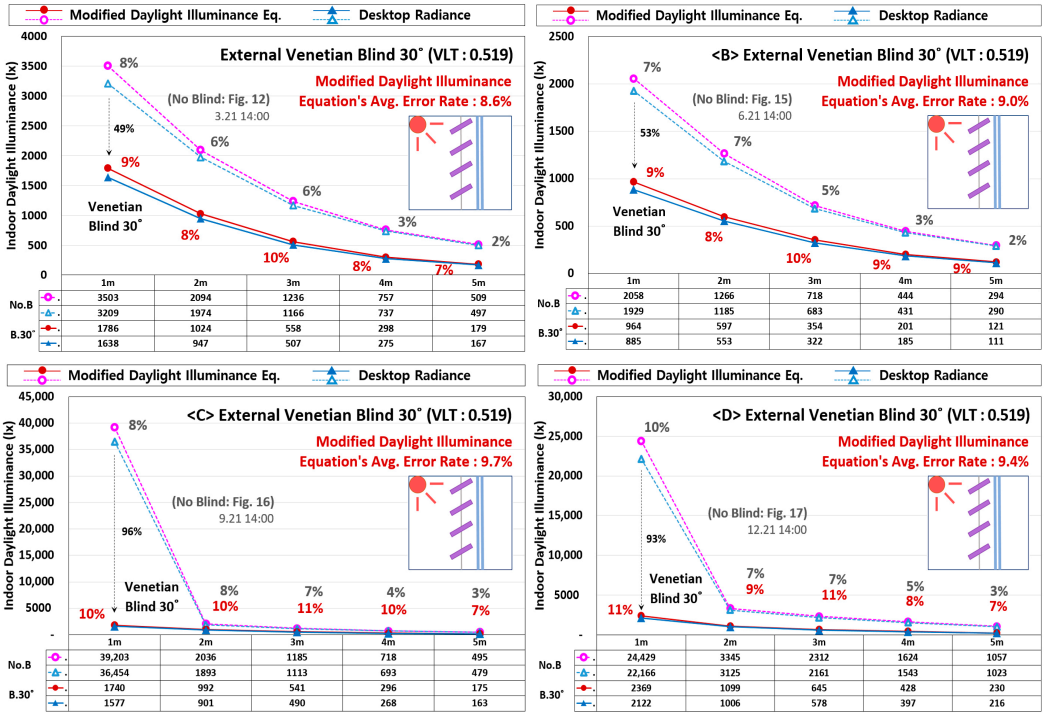

Figure 20. Comparison of indoor illuminance between the modified equation and Desktop Radiance simulation when installing external venetian blind 30° (**A**) 3.21 (**B**) 6.21 (**C**) 9.21 (**D**) 12.21 (14:00).

When installing external venetian blinds at 30°, the VLT was 0.519, which was calculated by using the Window 7.6 program [69]. When comparing illuminance prediction results of the Desktop Radiance simulation and modified prediction method, the error rates of 21st March were 9% at 1 m, 8% at 2 m, 10% at 3 m, 8% at 4 and 7% at 5 m. The average illuminance prediction error rate was 8.6%. The error rate was 9% at 1 m, 8% at 2 m, 10% at 3 m, 9% at 4 and 9% at 5 m on 21st June at 2:00 pm. On the 21st September and December, installing blinds blocked direct solar radiation to the 1m illuminance sensor and indoor illuminance at 1 m were reduced by 96% and 93%. When comparing illuminance prediction results of the Desktop Radiance simulation and modified prediction method, the average illuminance prediction error rate was 9.7% and 9.4%, respectively.

Figure 21 shows the results of a comparison between the Desktop Radiance simulation result and modified equations result in clear sky conditions (when installing blind 30°) for the entire day, excluding the night time, 07:00–18:00 (12 h).

When exterior venetian blind were installed at 30°, the Desktop Radiance simulation results and the proposed equation calculation results of the four seasonal representative dates showed high correlations satisfying the ASHRAE standards [63], all having a Pearson correlation coefficient R^2 value over 0.99, MBE value less than ±10% and Cv(RMSE) value less than 30%. The *t*-test results with significance level 0.05 showed a *p*-value less than 0.05. Therefore the Desktop Radiance simulation result and proposed daylight equation calculation result were showed to have statistical significance.

Tables S4-1, S4-2, S4-3, and S4-4 in the supplementary material provide detailed data for 21st March, 21st June, 21st September, and 21st December at 07:00–18:00 for Figure 21.

Figure 22 is a graph that compares the results of Desktop Radiance and the proposed prediction method when installing external venetian blinds at an angle of 45° on 21st March, 21st June, 21st September, and 21st December at 2:00 pm (CIE clear sky).

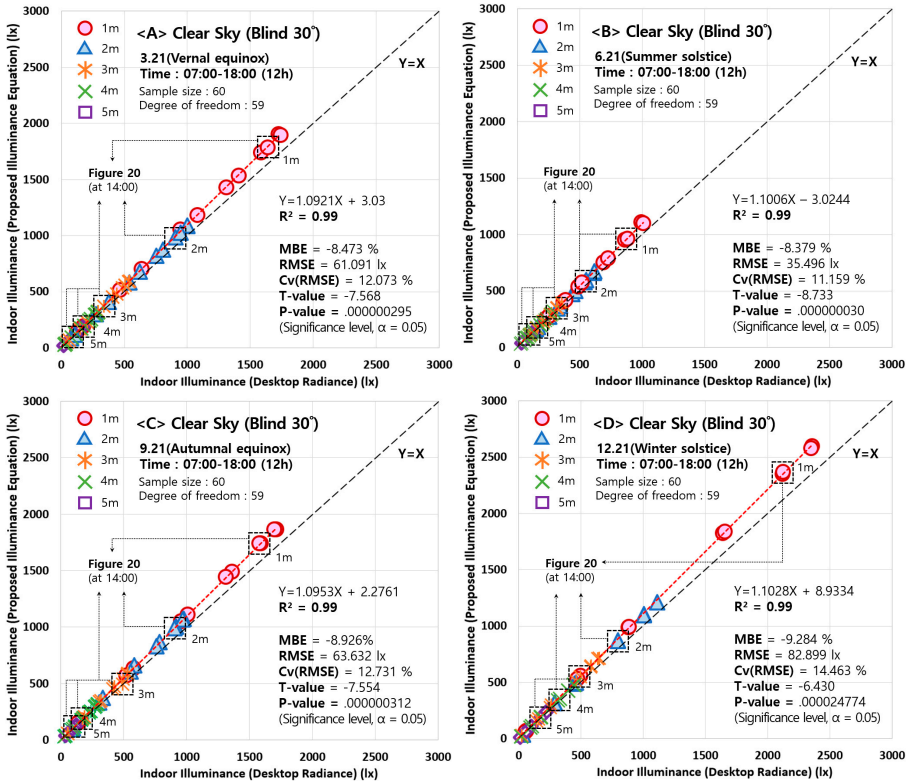

Figure 21. Comparison of indoor illuminance between the modified equation and Desktop Radiance in CIE clear sky when installing blind 30° (**A**) 3.21 (**B**) 6.21 (**C**) 9.21 (**D**) 12.21 (07:00–18:00).

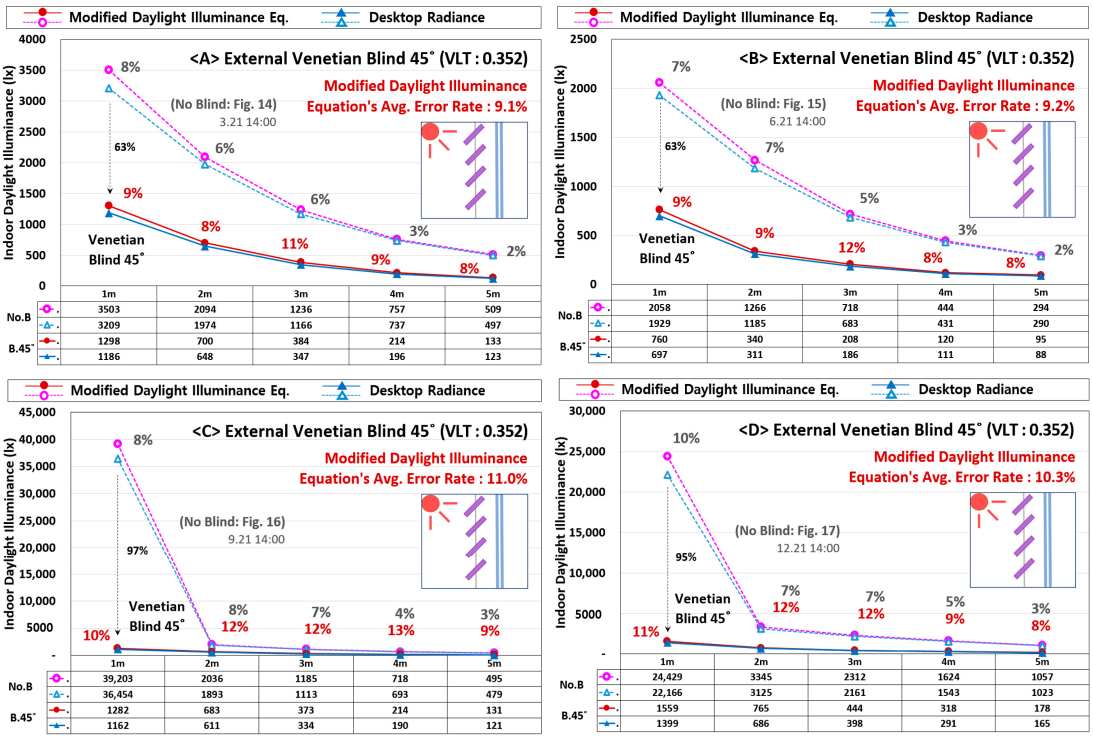

Figure 22. Comparison of indoor illuminance between the modified equation and Desktop Radiance simulation when installing external venetian blind 45° (**A**) 3.21 (**B**) 6.21 (**C**) 9.21 (**D**) 12.21 (14:00).

When installing external venetian blind at 45° on 21st March, 21st June, 21st September, and 21st December at 2:00 pm, the VLT was 0.352, which was calculated using the Window 7.6 program. When

comparing illuminance prediction results of the simulation and the modified prediction method, the error rates of 21st March were 9% at 1 m, 8% at 2 m, 11% at 3 m, 9% at 4 m, and 8% at 5 m. The average illuminance prediction error rate was 9.1%. The average illuminance prediction error rates of 21st June, 21st September, and 21st December at 2:00 pm were 9.2%, 11.0%, and 10.3%, respectively.

While Figure 22 shows detailed results at a specified time (14:00) on 21st March, 21st June, 21st September and 21st December, Figure 23 shows the results of a comparison between the Desktop Radiance simulation result and modified equations result in clear sky conditions for the entire day, excluding the night time, 07:00–18:00 (12 h).

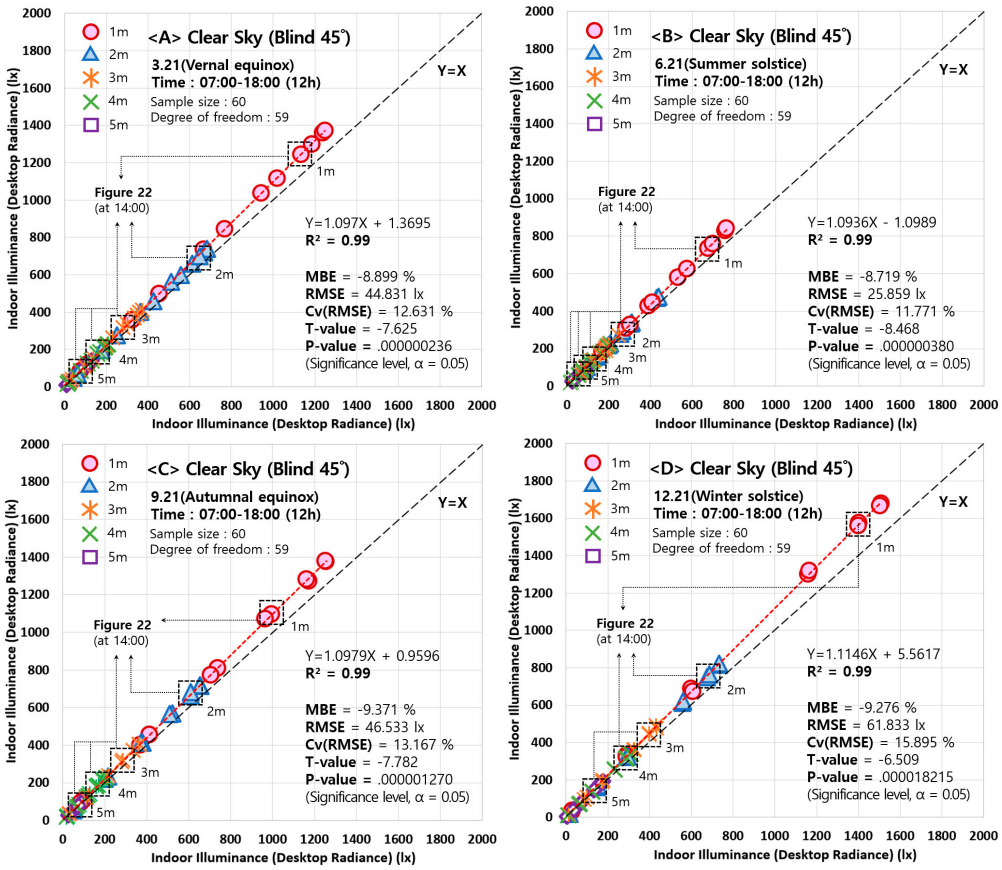

Figure 23. Comparison of indoor illuminance between the modified equation and Desktop Radiance simulation when installing external venetian blind 45° (**A**) 3.21 (**B**) 6.21 (**C**) 9.21 (**D**) 12.21 (07:00–18:00).

When exterior venetian blinds were installed at 45°, the Desktop Radiance simulation results and the proposed equation calculation results of the four seasonal representative dates showed a R^2 value over 0.99. The MBE for each seasonal representative date was lower than ±10% at −8.899%, −8.719%, −9.371%, and −9.276%. The Cv(RMSE) values were lower than 30% at 12.631%, 11.771%, 13.167%, and 15.895%, satisfying the ASHRAE standards [63]. *T*-test result showed that *p*-value were all lower than 0.05, indicating that Desktop Radiance simulation values and proposed daylight equation's calculated values possess statistical significance.

Tables S5-1, S5-2, S5-3, and S5-4 in the supplementary material provide detailed data for 21st March, 21st June, 21st September, and 21st December at 07:00–18:00 for Figure 23.

Figure 24 is a graph that compares the results of Desktop Radiance and the proposed prediction method when installing external venetian blinds at an angle of 60° on 21st March, 21st June, 21st September, and 21st December at 2:00 pm (CIE clear sky).

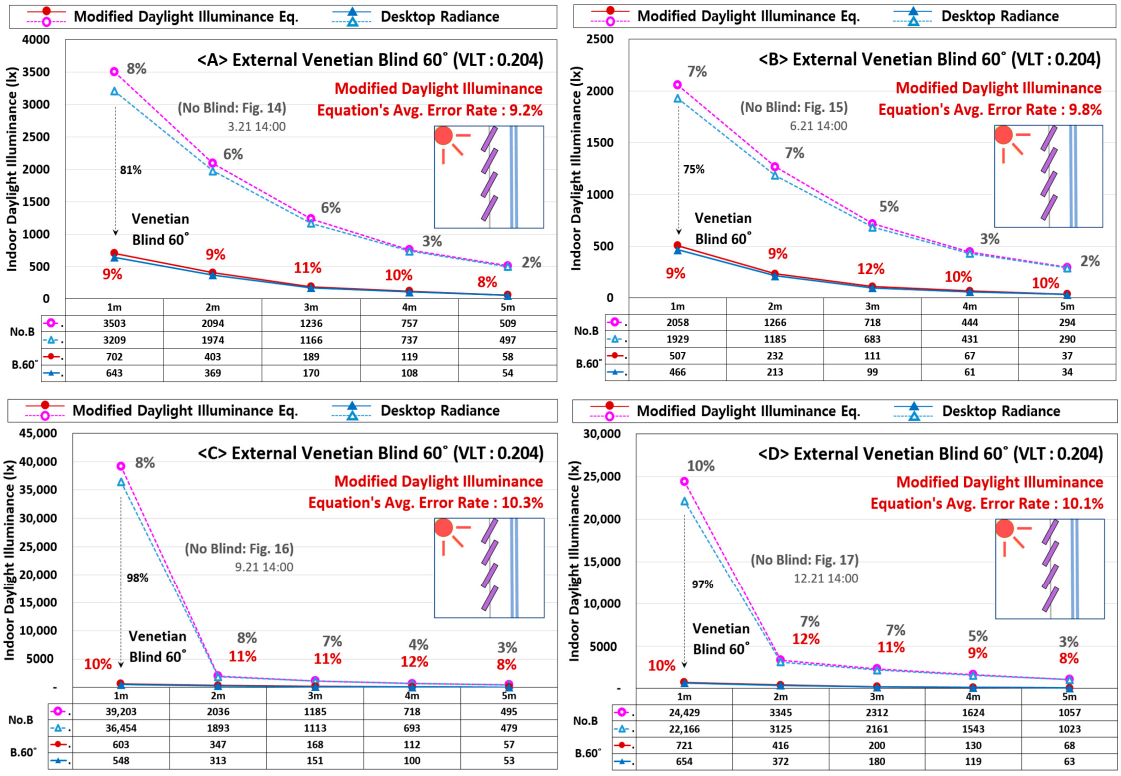

Figure 24. Comparison of indoor illuminance between the modified equation and Desktop Radiance simulation when installing external venetian blind 60° (**A**) 3.21 (**B**) 6.21 (**C**) 9.21 (**D**) 12.21 (14:00).

When installing external venetian blind at 60° on 21st March, 21st June, 21st September, and 21st December at 2:00 pm, VLT was 0.204, which was calculated using the Window 7.6 program. The VLT value decreased since the direct solar protection rate was higher than that when the slat angle was 45°. The illuminance distribution of slat angle 60° was also lower than that of the case with slat angles 30° and 45°. When comparing illuminance prediction result of the Desktop Radiance simulation and the prediction method, the error rates of 21st March were 9% at 1 m, 9% at 2 m, 11% at 3 m, 10% at 4 m, and 8% at 5 m. The average illuminance prediction error rate on 21st June, 21st September, 21st December at 2:00 pm were 9.8%, 10.3%, and 10.1%, respectively.

Figure 25 shows the results of a comparison between the Desktop Radiance simulation result and modified equations result in clear sky conditions (when installing blind 60°) for the entire day, excluding the night time, 07:00–18:00 (12 h).

We analyzed each luminance sensor's (1 m–5 m) Desktop Radiance simulation results and proposed equation calculation results via R^2, MBE, RMSE, Cv(RMSE) and performed the *t*-test (*t*-value, *p*-value). When blind was installed at 60°, all statistically analysis (R^2, MBE, Cv(RMSE), *t*-value, *p*-value) satisfied each standard and showed high correlations, just as when it was installed at 30° or 45°. It was possible to calculate indoor illuminance when installing the blinds, by substituting the variable value of VLT in the prediction method which is comparably accurate for the prediction of illuminance. Tables S6-1, S6-2, S6-3, and S6-4 in the Supplementary Material provide detailed data for 21st March, 21st June, 21st September, and 21st December at 07:00–18:00 for Figure 25.

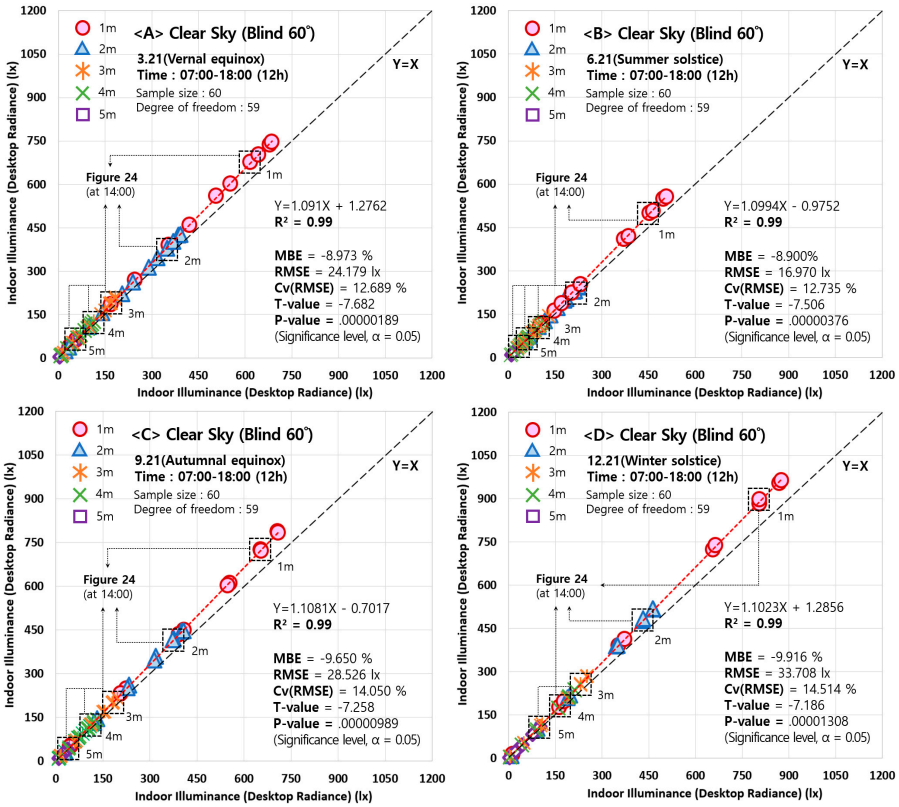

Figure 25. Comparison of indoor illuminance between the modified equation and Desktop Radiance simulation when installing external venetian blind 60° (**A**) 3.21 (**B**) 6.21 (**C**) 9.21 (**D**) 12.21 (07:00–18:00).

6. Summary and Conclusions

In this study, an algorithm framework for sky luminance distribution was first designed through theoretical considerations of the CIE general sky model. This was done in order to enable illuminance predictions without using high–cost facilities, realize the sky luminance distribution of CIE overcast sky and CIE clear sky conditions, and verify these findings through a comparison with the Desktop Radiance simulation results. This study then proposed and evaluated the modified illuminance prediction method by considering the effects of sky luminance, direct solar radiation, and reflective wall components and suggested a method to accurately predict indoor daylight illuminance during the initial building design phase for lighting energy conservation. The conclusions that can be drawn from this study are listed below:

(1) The CIE sky luminance distribution can be calculated using the location of the sun and the sky elements, the parameters of the CIE general sky model, and 145 sky patches. These luminance values can be applied to sky patches to reproduce the sky luminance distribution of each sky (CIE overcast sky and CIE clear sky).

(2) When the CIE sky luminance algorithm's calculation results were compared with Desktop Radiance simulation's sky luminance value, on the two sky types with four seasonal representative dates (21st March, 21st June, 21st September, and 21st December), four directions (North, South, East and West) on five locations (A–E), the Pearson correlation coefficient R^2 over 0.99, MBE value and Cv (RMSE) value, showing a high correlation satisfying the ASHRAE guidelines. The *t*-test results with significance level 0.05 showed a *p*-value less than 0.05. Therefore, the calculation results from the algorithm framework of CIE sky luminance distribution have statistical significance with the Desktop Radiance Simulation results. When sky luminance algorithm was used, its predictability was evaluated to be rather accurate when compared with Desktop Radiance simulation results.

(3) The DeLight algorithm was analyzed and a modified illuminance prediction method was suggested. Illuminance that was calculated by the modified prediction method result was compared with Desktop Radiance simulation result when its CIE overcast sky. The simulation results and the proposed equation calculation results of the four seasonal representative dates showed high correlations, all having the R^2 value over 0.99, MBE value less than ±10% and Cv(RMSE) value less than 30%. The *t*-test results with a significance level of 0.05 showed a *p*-value of less than 0.05. Therefore, this study verified that the suggested equation can be utilized in the overcast sky.

(4) This study evaluated DF by classifying component into SC and IRC. DF was calculated by the modified prediction method and Desktop Radiance simulation when its CIE overcast sky. As a result DF can be evaluated by SC and IRC since there is no significant difference between the modified prediction method and simulation values. All statistical analysis (R^2, MBE, Cv(RMSE), *t*-test) satisfied each standard and showed high correlations.

(5) Predicting illuminance when its CIE clear sky, it is important that there are solar radiation influxes hitting the building. Due to this reason, this study unfolds the simulation model into six sides and has also checked the indoor illuminance distribution. The correlation of Desktop Radiance simulation results and the proposed equation calculation results of the four seasonal representative dates showed a R^2 value over 0.99. The MBE for each seasonal representative date (21st March, 21st June, 21st September, and 21st December) was lower than ±10% at −8.899%, −8.719%, −9.371%, and −9.276%. The Cv(RMSE) values were lower than 30% at 12.631%, 11.771%, 13.167%, and 15.895%, satisfying the ASHRAE standards. The *t*-test results showed that the *p*-value were all lower than 0.05. The simulation values and proposed daylight equation's calculated the values that all possessed a statistical significance.

(6) Additionally, when the exterior venetian blinds were installed at 30°, 45° and 60°, this study compared the simulation illuminance value of the Radiance program and the calculation value of the proposed equation. All statistical analysis (R^2, MBE, Cv(RMSE), *t*-test) satisfied each standard and showed high correlations. It was possible to calculate indoor illuminance when installing the solar shading system, by substituting the variable value of VLT in the prediction method, which is comparably accurate for the prediction of illuminance.

(7) By verifying the accuracy of the developed prediction method for calculating indoor illuminance, prediction was deemed possible even when there were changes in the sky conditions, sun location, and blind slat angle. However, it is also necessary to study the factors influencing indoor illumination prediction. The study will proceed considering real experimental case study, the positional direction of the study model, blind control, lighting system control strategy, and influence of surrounding buildings on indoor illumination prediction.

Supplementary Materials: The following are available online at http://www.mdpi.com/1996-1073/12/4/592/s1, Table S1-1, S1-2, S1-3, and S1-4. Prediction results and statistical analysis of indoor daylight illuminance in CIE overcast sky using by Desktop Radiance (3.21 at 07:00 am–06:00 pm), (6.21 at 07:00 am–06:00 pm), (9.21 at 07:00 am–06:00 pm), and (12.21 at 07:00 am–06:00 pm), Table S2-1, S2-2, S2-3, and S2-4. Prediction results and statistical analysis of daylight factor (sky component and internally reflected component) in CIE overcast sky using by Desktop Radiance (3.21 at 07:00 am–06:00 pm), (6.21 at 07:00 am–06:00 pm), (9.21 at 07:00 am–06:00 pm), and (12.21 at 07:00 am–06:00 pm), Table S3-1, S3-2, S3-3, and S3-4. Prediction results and statistical analysis of indoor daylight illuminance in CIE clear sky using by Desktop Radiance (3.21 at 07:00 am–06:00 pm), (6.21 at 07:00 am–06:00 pm), (9.21 at 07:00 am–06:00 pm), and (12.21 at 07:00 am–06:00 pm), Table S4-1, S4-2, S4-3, and S4-4. Prediction results and statistical analysis of indoor daylight illuminance in CIE clear sky (installing external venetian blind 30°) using by Desktop Radiance (3.21 at 07:00 am–06:00 pm), (6.21 at 07:00 am–06:00 pm), (9.21 at 07:00 am–06:00 pm), and (12.21 at 07:00 am–06:00 pm), Table S5-1, S5-2, S5-3, and S5-4. Prediction results and statistical analysis of indoor daylight illuminance in CIE clear sky (installing external venetian blind 45°) using by Desktop Radiance (3.21 at 07:00 am–06:00 pm), (6.21 at 07:00 am–06:00 pm), (9.21 at 07:00 am–06:00 pm), and (12.21 at 07:00 am–06:00 pm) Table S6-1, S6-2, S6-3, and S6-4. Prediction results and statistical analysis of indoor daylight illuminance in CIE clear sky (installing external venetian blind 60°) using by Desktop Radiance (3.21 at 07:00 am–06:00 pm), (6.21 at 07:00 am–06:00 pm), (9.21 at 07:00 am–06:00 pm), and (12.21 at 07:00 am–06:00 pm).

Author Contributions: C.-H.K. performed the simulation and data analysis, and wrote this paper based on the obtained results. K.-S.K. led and supervised this study. All of the authors have contributed for collecting ideas and concepts presented in the paper.

Funding: This research was supported by Basic Science Research Program through the National Research Foundation of Korea (NRF) funded by the Ministry of Education (No. 2017R1D1A1B03028205).

Conflicts of Interest: The authors declare no conflict of interest.

Abbreviations

The following abbreviations are used in this manuscript:

ALT	Altitude
AM	Ante Meridiem
ASHRAE	American Society of Heating, Refrigerating and Air–Conditioning Engineers
AVG	Average Value
AZI	Azimuth
CIE	Commission Internationale de l'Eclairage (International Commission on Illuminance)
Cv(RMSE)	Coefficient of Variance of the Root Mean Square Error
DF	Daylight Factor
DOE	U.S.A. Department of Energy
EHI	Exterior Horizontal Illuminance
IRC	Internally Reflected Component
ISO	International Organization for Standardization
LBNL	Lawrence Berkeley National Laboratory
PM	Post Meridiem
MAX	Maximum Value
MBE	Mean Bias Error
MIN	Minimum Value
RMSE	Root Mean Square Error
SC	Sky Component
VLT	Visible Light Transmittance
WWR	Window to Wall Area Ratio

References

1. Nabil, A.; Mardaljevic, J. Useful daylight illuminance: A new paradigm for assessing daylight in buildings. *Light. Res. Technol.* **2005**, *37*, 41–57.
2. Li, D.H. A review of daylight illuminance determinations and energy implications. *Appl. Energy* **2010**, *87*, 2109–2118. [CrossRef]
3. Pérez-Lombard, L.; Ortiz, J.; Pout, C. A review on buildings energy consumption information. *Energy Build.* **2008**, *40*, 394–398. [CrossRef]
4. Amasyali, K.; El-Gohary, N.M. A review of data–driven building energy consumption prediction studies. *Renew. Sustain. Energy Rev.* **2018**, *81*, 1192–1205. [CrossRef]
5. Kaminska, A.; Ożadowicz, A. Lighting Control Including Daylight and Energy Efficiency Improvements Analysis. *Energies* **2018**, *11*, 2166. [CrossRef]
6. Kim, C.H.; Lee, S.E.; Kim, K.S. Analysis of Energy Saving Potential in High–Performance Building Technologies under Korean Climatic Conditions. *Energies* **2018**, *11*, 884. [CrossRef]
7. Roisin, B.; Bodart, M.; Deneyer, A.; D'herdt, P. Lighting energy savings in offices using different control systems and their real consumption. *Energy Build.* **2008**, *40*, 514–523. [CrossRef]
8. De Bakker, C.; van de Voort, T.; Rosemann, A. The energy saving potential of occupancy–based lighting control strategies in open–plan offices: the influence of occupancy patterns. *Energies* **2017**, *11*, 2. [CrossRef]
9. Acosta, I.; Campano, M.; Domínguez-Amarillo, S.; Muñoz, C. Dynamic Daylight Metrics for Electricity Savings in Offices: Window Size and Climate Smart Lighting Management. *Energies* **2018**, *11*, 3143. [CrossRef]
10. Igawa, N. Improving the All Sky Model for the luminance and radiance distributions of the sky. *Sol. Energy* **2014**, *105*, 354–372. [CrossRef]

11. Kittler, R.; Darula, S. Scattered sunlight determining sky luminance patterns. *Renew. Sustain. Energy Rev.* **2016**, *62*, 575–584. [CrossRef]
12. Li, D.H.; Lou, S.; Ghaffarianhoseini, A.; Alshaibani, K.A.; Lam, J.C. A review of calculating procedures on daylight factor based metrics under various CIE Standard Skies and obstructed environments. *Build. Environ.* **2017**, *112*, 29–44. [CrossRef]
13. Alshaibani, K. Average daylight factor for the ISO/CIE Standard General Sky. *Light. Res. Technol.* **2016**, *48*, 742–754.
14. Commission Internationale de l'Eclairage, International Commission on Illuminance (CIE). Available online: http://www.cie.co.at/publications/spatial-distribution-daylight-cie-standard-general-sky (accessed on 6 January 2019).
15. Darula, S.; Kittler, R. CIE general sky standard defining luminance distributions. In Proceedings of the 2002 IBPSA Conference (Proceedings eSim), Montreal, QC, Canada, 12 September 2002; International Building Performance Simulation Association (IBPSA). Available online: http://www.ibpsa.org/?page_id=291 (accessed on 6 January 2019).
16. Verso, V.R.L.; Pellegrino, A.; Serra, V. Light transmission efficiency of daylight guidance systems: An assessment approach based on simulations and measurements in a sun/sky simulator. *Sol. Energy* **2011**, *85*, 2789–2801. [CrossRef]
17. Michel, L.; Scartezzini, J.L. Implementing the partial daylight factor method under a scanning sky simulator. *Sol. energy* **2002**, *72*, 473–492. [CrossRef]
18. Maskarenj, M.; Chawla, G.; Banerjee, R.; Ghosh, P.C. Evaluation of dynamic sky–type using novel angular sky luminance measurement system. *Build. Environ.* **2018**, *146*, 152–165. [CrossRef]
19. Hosek, L.; Wilkie, A. An analytic model for full spectral sky-dome radiance. *ACM Trans. Graph. (TOG)* **2012**, *31*, 95. [CrossRef]
20. ISO (the International Organization for Standardization). *Spatial distribution of daylight—CIE standard general sky*; 15469:2004(en); International Commission on Illumination (CIE): Vienna, Austria, 2004.
21. Darula, S.; Ashdown, I.; Bartzokas, A.; Bisegna, F.; Dumortier, D.; Greenup, P.; Kambezidis, H.D.; Kendrick, D.; Kittler, R.; Kobav, M.; et al. *CIE Standard General Sky Guide, CIE 215:2014*; International Commission on Illumination (CIE): Vienna, Austria, 2014.
22. Kittler, R.; Darula, S. The simultaneous occurrence and relationship of sunlight and skylight under ISO/CIE standard sky types. *Light. Res. Technol.* **2015**, *47*, 565–580.
23. Darula, S.; Kittler, R. A methodology for designing and calibrating an artificial sky to simulate ISO/CIE sky types with an artificial sun. *Leukos* **2015**, *11*, 93–105. [CrossRef]
24. Darula, S.; Kittler, R. New trends in daylight theory based on the new ISO/CIE Sky Standard: 1. Zenith luminance on overcast skies. *Build. Res. J.* **2004**, *52*, 181–197.
25. Kittler, R.; Darula, S. The method of aperture meridians: a simple calculation tool for applying the ISO/CIE Standard General Sky. *Light. Res. Technol.* **2006**, *38*, 109–119.
26. Lawrence Berkeley National Laboratory (LBNL), Building Technologies Department, Desktop Radiance Program. Available online: http://radsite.lbl.gov/deskrad/links.htm (accessed on 6 January 2019).
27. Michael, A.; Gregoriou, S.; Kalogirou, S.A. Environmental assessment of an integrated adaptive system for the improvement of indoor visual comfort of existing buildings. *Renew. Energy* **2018**, *115*, 620–633. [CrossRef]
28. Vassiliades, C.; Michael, A.; Savvides, A.; Kalogirou, S. Improvement of passive behaviour of existing buildings through the integration of active solar energy systems. *Energy* **2018**, *163*, 1178–1192. [CrossRef]
29. Zhu, T.; Li, R.; Li, C. The Analysis of Natural Lighting Simulation and Study on Energy Saving in Cigarette Factory. *Procedia Eng.* **2017**, *205*, 895–901. [CrossRef]
30. Hellinga, H.; Hordijk, T. The D&V analysis method: A method for the analysis of daylight access and view quality. *Build. Environ.* **2014**, *79*, 101–114.
31. Vartiainen, E. *Daylight modelling with the simulation tool DeLight*; Technical Report TKK-F-A799; Engineering Physics and Mathematics, Helsinki University of Technology: Helsinki, Finland, 2000.
32. Vartiainen, E.; Peippo, K.; Lund, P. Daylight optimization of multifunctional solar facades. *Sol. Energy* **2000**, *68*, 223–235. [CrossRef]
33. Hitchcock, R.; Carroll, W. DElight: a daylighting and electric lighting simulation engine. In Proceedings of the Eighth International IBPSA Conference, Eindhoven, The Netherlands, 11–14 August 2003.

34. U.S. Department of Energy (DOE). *EnergyPlus Engineering Reference (Version 8.8.0 Documentation; Building Technologies Program)*; U.S. Department of Energy: Washington, DC, USA, 2017.
35. Tregenza, P.R. Standard skies for maritime climates. *Int. J. Light. Res. Technol.* **1999**, *31*, 97–106. [CrossRef]
36. Tregenza, P.R. Analyzing sky luminance scans to obtain frequency distributions of CIE Standard General Skies. *Light. Res. Technol.* **2004**, *36*, 271–279.
37. Enarun, D.; Littlefair, P. Luminance models for overcast skies: assessment using measured data. *Int. J. Light. Res. Technol.* **1995**, *27*, 53–58. [CrossRef]
38. Li, D.H.; Lau, C.C.; Lam, J.C. A study of 15 sky luminance patterns against Hong Kong data. *Archit. Sci. Rev.* **2003**, *46*, 61–68. [CrossRef]
39. Li, D.H.; Lau, C.C.; Lam, J.C. Overcast sky conditions and luminance distribution in Hong Kong. *Build. Environ.* **2004**, *39*, 101–108. [CrossRef]
40. Chirarattananon, S.; Chaiwiwatworakul, P. Distributions of sky luminance and radiance of North Bangkok under standard distributions. *Renew. Energy* **2007**, *32*, 1328–1345. [CrossRef]
41. Igawa, N.; Koga, Y.; Matsuzawa, T.; Nakamura, H. Models of sky radiance distribution and sky luminance distribution. *Sol. Energy* **2004**, *77*, 137–157. [CrossRef]
42. Li, D.H.; Lau, C.C. An analysis of nonovercast sky luminance models against Hong Kong data. *J. Sol. Energy Eng.* **2007**, *129*, 486–493. [CrossRef]
43. Bartzokas, A.; Kambezidis, H.D.; Darula, S.; Kittler, R. Comparison between winter and summer sky–luminance distribution in Central Europe and in the Eastern Mediterranean. *J. Atmos. Sol. Terr. Phys.* **2005**, *67*, 709–718. [CrossRef]
44. Wittkopf, S.K.; Soon, L.K. Analysing sky luminance scans and predicting frequent sky patterns in Singapore. *Light. Res. Technol.* **2007**, *39*, 31–51.
45. Love, J.A.; Navvab, M. Daylighting estimation under real skies: a comparison of full–scale photometry, model photometry, and computer simulation. *J. Illum. Eng. Soc.* **1991**, *20*, 140–156. [CrossRef]
46. Navvab, M. Scale model photometry techniques under simulated sky conditions. *J. Illum. Eng. Soc.* **1996**, *25*, 160–172. [CrossRef]
47. Navvab, M.; Perez, R.; Hosobuchi, H. The Estimated Frequencies of CIE Luminance Distributions and the Impact of Circumsolar Region Using TMY Weather Files. In Proceedings of the 43rd ASES National Solar Conference 2014, SOLAR 2014, Including the 39th National Passive Solar Conference and the 2nd Meeting of Young and Emerging Professionals in Renewable Energy, San Francisco, CA, USA, 6–10 July 2014.
48. Gugliermetti, F.; Bisegna, F. Daylighting with external shading devices: design and simulation algorithms. *Build. Environ.* **2006**, *41*, 136–149. [CrossRef]
49. Gugliermetti, F.; Bisegna, F. A model study of light control systems operating with Electrochromic Windows. *Light. Res. Technol.* **2005**, *37*, 3–19.
50. Tregenza, P.R. Modification of the split–flux formulae for mean daylight factor and internal reflected component with large external obstructions. *Light. Res. Technol.* **1989**, *21*, 125–128.
51. Tregenza, P.R. Mean daylight illuminance in rooms facing sunlit streets. *Build. Environ.* **1995**, *30*, 83–89. [CrossRef]
52. Li, D.H.W.; Cheung, G.H.W.; Cheung, K.L. Evaluation of simplified procedure for indoor daylight illuminance determination against data in scale model measurements. *Indoor Built Environ.* **2006**, *15*, 213–223. [CrossRef]
53. Li, D.H.W.; Lau, C.C.S.; Lam, J.C. Predicting daylight illuminance by computer simulation techniques. *Light. Res. Technol.* **2004**, *36*, 113–128.
54. Yoon, K.C.; Yun, S.I.; Kim, S.S.; Kim, K.S. Application of simplified daylight prediction method for daylighting performance evaluation on overcast sky. *J. Korean Sol. Energy Soc.* **2014**, *34*, 1–9. [CrossRef]
55. Moon, P.; Spencer, D.E. Illumination from a non-uniform sky. *Trans. Illum. Eng. Soc.* **1942**, *37*, 707–726.
56. Kittler, R. Standardization of outdoor conditions for the calculation of daylight factor with clear skies. In Proceedings of the CIE International Conference on Sunlight in Buildings, Rotterdam, The Netherlands, 5–9 April 1967; International Commission on Illumination (CIE): Vienna, Austria, 1967; pp. 273–285.
57. Bryan, H.J.; Clear, R.D. Calculating interior daylight illumination with a programmable hand calculator. *J. Illum. Eng. Soc.* **1981**, *10*, 219–227. [CrossRef]
58. Korean Ministry of Land, Infrastructure and Transport (MOLIT). *Window design Guidelines for Building Energy Conservation*; MOLIT: Sejong-si, Korea, 2012.

59. Ghisi, E.; Tinker, J.A. An ideal window area concept for energy efficient integration of daylight and artificial light in buildings. *Build. Environ.* **2005**, *40*, 51–61. [CrossRef]
60. Kim, C.H.; Kim, K.S. Evaluation of thermal and visual environment for the glazing and shading device in an office building with installed of venetian blind. *Korea Inst. Ecol. Archit. Environ.* **2015**, *15*, 101–109. [CrossRef]
61. Kim, C.H.; Kim, K.S. A Study on Prediction Method of Sky Luminance Distributions for CIE Overcast Sky and CIE Clear Sky. *J. Korean Sol. Energy Soc.* **2016**, *36*, 33–43. [CrossRef]
62. Lee Rodgers, J.; Nicewander, W.A. Thirteen ways to look at the correlation coefficient. *Am. Stat.* **1988**, *42*, 59–66. [CrossRef]
63. Department of Energy (DOE). *M&V Guidelines Measurement and Verification for Federal Energy Projects*; DOE of Energy Efficiency and Renewable Energy: Washington, DC, USA, 2000.
64. Psiloglou, B.E.; Kambezidis, H.D. Estimation of the ground albedo for the Athens area, Greece. *J. Atmos. Sol. Terr. Phys.* **2009**, *71*, 943–954. [CrossRef]
65. DIN Standards Committee Lighting Technology, Daylight in buildings; EN 17037:2018. Available online: https://www.din.de/en/getting-involved/standards-committees/fnl/projects/wdc-proj:din21:234133788 (accessed on 18 January 2019).
66. Mangione, A.; Mattoni, B.; Bisegna, F.; Iatauro, D.; Zinzi, M. On the Validity of Daylight Factor for Evaluating the Energy Performance of Building. In Proceedings of the 2018 IEEE International Conference on Environment and Electrical Engineering and 2018 IEEE Industrial and Commercial Power Systems Europe (EEEIC/I&CPS Europe), Palermo, Italy, 12–15 June 2018.
67. Li, D.H.W.; Cheung, G.H.W. Average daylight factor for the 15 CIE standard skies. *Light. Res. Technol.* **2006**, *38*, 137–149.
68. Sudan, M.; Tiwari, G.N.; Al-Helal, I.M. A daylight factor model under clear sky conditions for building: An experimental validation. *Sol. Energy* **2015**, *115*, 379–389. [CrossRef]
69. Energy Technologies Area Lawrence Berkeley National Laboratory, Building Technology & Urban Systems Division, Windows and Daylighting. Available online: https://windows.lbl.gov/tools/window/software-download (accessed on 6 January 2019).